Electronic Supplementary Information

A Record-High EQE of 7.65%@3300 cd m^{-2} Achieved in Non-Doped Near-Ultraviolet OLEDs Based on Novel D'-D-A Type Bipolar Fluorophores upon Molecular Configuration Engineering

Haoyuan Qi,[a] Danyu Xie,[b] Zexuan Gao,[a] Shengnan Wang,[a] Ling Peng,[c] Yuchao Liu,[a] Shian Ying,*[a] Dongge Ma*[b] and Shouke Yan*[a, d]

[a] Key Laboratory of Rubber-Plastics, Ministry of Education, Qingdao University of Science & Technology, Qingdao 266042, P. R. China.

[b] Center for Aggregation-Induced Emission, Institute of Polymer Optoelectronic Materials and Devices, State Key Laboratory of Luminescent Materials and Devices, South China University of Technology, Guangzhou 510640, P. R. China.

[c] College of Chemistry and Chemical Engineering, Heze University, Heze 274015, P. R. China.

[d] State Key Laboratory of Chemical Resource Engineering, College of Materials Science and Engineering, Beijing University of Chemical Technology, Beijing 100029, P. R. China.

E-mail: shian0610@126.com (S. Ying); msdgma@scut.edu.cn (D. Ma); skyan@mail.buct.edu.cn (S. Yan)

1. Experimental Methods

1.1. Experimental measurements

^{1}H and ^{13}C nuclear magnetic resonance (NMR) spectra were performed by the Bruker AC400 spectrometer at 400 MHz and 100 MHz with $CDCl_3$ and tetramethylsilane (TMS) as the solvent and internal standard, respectively. Mass spectra of compound were measured by High Resolution Quadrupole Time of Flight Tandem Mass Spectrometer (TOF-MS). Ultraviolet-visible absorption and emission spectra were carried out by using Hitachi U-2910 absorption spectrometer and Hitachi F-4700 spectrophotometer, respectively. Photoluminescence quantum yields (PLQYs) of materials in solution and film were estimated by using the integration sphere setup (Hamamatsu C11347-11) equipped with a xenon high-pressure lamp and a multichannel analyzer from 200 to 950 nm. Fluorescence lifetimes were determined on a FLS1000 transient fluorescence spectrometer with an EPL-340 optical laser. Thermogravimetric analysis (TGA) curves of materials were performed using a Netzsch (209F1) thermogravimetric analyzer under a nitrogen atmosphere (50 mL min^{-1}) at a heating rate of 10 ^{o}C min^{-1}. Differential scanning calorimetry (DSC) curves of target compounds were recorded by a Netzsch DSC (204F1) instrument at a heating (or cooling) rate of 10 ℃ min^{-1}. Cyclic voltammetry (CV) was measured on a CHI660E electrochemical workstation in a conventional three-electrode system including a glass carbon working electrode, a platinum wire auxiliary electrode, and an Ag/Ag^{+} standard reference electrode, where tetrabutylammonium hexafluorophosphate (Bu_4NPF_6, 0.1 M) in anhydrous dichloromethane acted as the supporting electrolyte and ferrocene served as the standard reference. The HOMO energy level (E_{HOMO}) and the LUMO energy level (E_{LUMO}) can be calculated by the following **Equation 1 and 2**:

$$E_{HOMO} = -(E_{OX} - E_{\frac{1}{2}}^{+} + 4.8) \quad (1)$$

$$E_{LUMO} = E_{HOMO} + E_g \quad (2)$$

Here, E_{OX} is the oxidation onset potential. $E_{\frac{1}{2}}^{+}$ is the half wave potential of Fc^+/Fc. E_g was the optical bandgap evaluated from the onset of absorption spectrum.

1.2. Theoretical calculations

All the density functional theory (DFT) and time dependent DFT (TD-DFT) calculations were carried out using Gaussian 16 A.03 package. The optimized ground-state geometries, energy levels, and frontier molecular orbital (FMO) distributions were calculated on the basis of DFT by using B3LYP/6-31G(d, p) method. The geometry of the lowest singlet excited state (S_1 state) was optimized by TD-DFT at the B3LYP/6–31G(d, p) level. Multifwn 3.8 was utilized to analyze the natural transition orbitals (NTOs) of excited states.[24] Spin-orbit coupling (SOC) matrix elements were calculated by TD-DFT and the ORCA 4.1.1 package at B3LYP/6-31G(d, p). [25]

1.3. Device fabrication and measurement

Patterned indium-tin-oxide (ITO) glasses with a sheet resistance of 20 Ω per square were ultrasonically treated in detergents and deionized water, then dried for 30 mins at 120 °C. After treated by oxygen plasma for 7 mins, Clean ITO substrates were transferred into the vacuum deposition system. The target compounds used for device have been sublimated. When the pressure less than 2×10^{-4} Pa, the devices were fabricated. The evaporation rates of organic materials, lithium fluoride (LiF) and aluminum (Al) were 1-1.5, 0.2 and 5-10 Å s^{-1} via a shadow mask, which were detected by a frequency counter and calibrated by a Dektak 6 M profiler (Veeco). The emitting area (3×3 mm^2) was determined by the overlap between ITO and Al electrodes. The current density–luminance–voltage characteristics were performed by the computer controlled Keithley 2450 Series Digital Source-meter and LS160 Luminancemeter (KONICAMINOLTA). EL spectra at different voltages were recorded by the optical analyzer

FlAME-S-VIS-NIR photometer. Supposing the light emitted by the devices accorded with the Lambertian distribution, the EQEs can be calculated from the EL spectra, luminance, and current density.

1.4 Synthesis and characterization

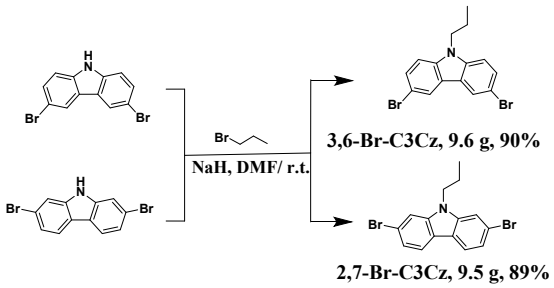

Scheme S1. Synthetic route of **3,6-Br-C3Cz** and **2,7-BrC3Cz**.

Synthesis of 3,6-dibromo-9-propyl-9*H*-carbazole (3,6-Br-C3Cz): Under nitrogen atmosphere, 3,6-dibromo-9*H*-carbazole (9.5 g, 29.2 mmol), *N,N*-dimethylformamide (DMF, 80 mL) were added into a 250 mL two-neck round-bottom flask with the ice-water bath for 0.5 h. Sodium hydride (1.1 g, 43.8 mmol) divided into 4 times was added within 2 h. Then 1-bromopropane (2.9 mL, 32.1 mmol) was added. After reacted for 6 h at room temperature, the reaction mixture was extracted three times with CH_2Cl_2 and water. The organic layer was dried with anhydrous $MgSO_4$, filtered, and evaporated under reduced pressure. The crude product was purified by silica-gel column chromatography using petroleum / CH_2Cl_2 (8/1, v/v) as the eluant. Finally, a white solid was obtained (9.6 g, 90%). ^{1}H NMR (400 MHz, $CDCl_3$) δ 8.11 (d, J = 1.9 Hz, 2H), 7.53 (dd, J = 8.7, 1.9 Hz, 2H), 7.27 – 7.23 (m, 2H), 4.19 (t, J = 7.1 Hz, 2H), 1.86 (q, J = 7.3 Hz, 2H), 0.92 (t, J = 7.4 Hz, 3H). ^{13}C NMR (101 MHz, $CDCl_3$) δ 139.40, 129.01, 123.44, 123.25, 111.95, 110.44, 77.36, 77.04, 76.72, 44.87, 22.23, 11.73.

Synthesis of 2,7-dibromo-9-propyl-9*H*-carbazole (2,7-Br-C3Cz): The synthetic procedure of **2,7-Br-C3Cz** is similar to that of **3,6-Br-C3Cz** with 2,7-dibromo-9*H*-carbazole

(9.5 g, 29.1 mmol) and 1-bromopropane (2.9 mL, 32.1 mmol) as raw materials. Finally, a white solid was obtained (9.5 g, 89%).^{1}H NMR (400 MHz, $CDCl_3$) δ 7.76 (d, *J* = 8.2 Hz, 2H), 7.42 (d, *J* = 1.6 Hz, 2H), 7.23 (dd, *J* = 8.3, 1.6 Hz, 2H), 4.04 (t, *J* = 7.3 Hz, 2H), 1.78 (h, *J* = 7.4 Hz, 2H), 0.88 (t, *J* = 7.4 Hz, 3H). ^{13}C NMR (101 MHz, $CDCl_3$) δ 141.39, 122.52, 121.46, 121.25, 119.70, 112.02, 77.42, 77.11, 76.79, 44.83, 22.16, 11.73.

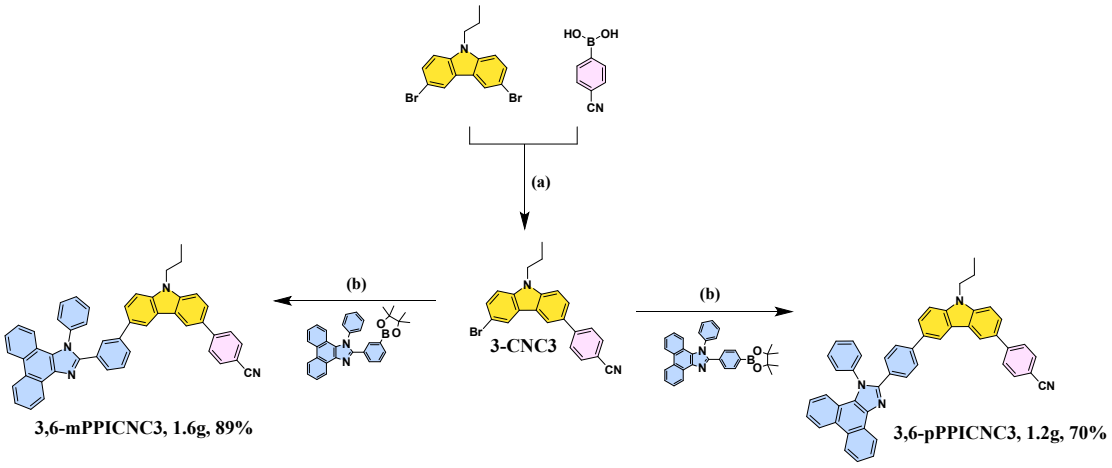

Scheme 2. Synthetic routes to **3,6-mPPICNC3** and **3,6-pPPICNC3**. (a) $Pd(PPh_3)_4$, K_2CO_3 (2M), THF, 75 ℃, 18 h. (b). $Pd(PPh_3)_4$, K_2CO_3 (2M), THF, 80 ℃, 24 h.

Synthesis of 4-(6-bromo-9-propyl-9*H*-carbazol-3-yl)benzonitrile (3-CNC3): Under nitrogen atmosphere, **3,6-Br-C3Cz** (8.0 g, 22.0 mmol), (4-cyanophenyl)boronic acid (1.6 g, 11.0 mmol), and tetrakis(triphenylphosphine)palladium ($Pd(PPh_3)_4$, 0.5 g, 0.4 mmol) were placed in a 250 mL two-neck round-bottom flask. Then tetrahydrofuran (THF, 60 mL), 2 M potassium carbonate (10 mL) were injected into the flask. The reaction mixture was stirred and refluxed at 75 ℃ for 18 h. After cooling to room temperature, the reaction mixture was extracted 3 times with CH_2Cl_2 and water. The organic layer was dried with anhydrous $MgSO_4$, filtered, and evaporated under reduced pressure. The crude product was purified by silica-gel column chromatography using petroleum / CH_2Cl_2 (4/1, v/v) as the mixed eluant, giving a white solid (2.1 g, 49%). ^{1}H NMR (400 MHz, $CDCl_3$) δ 8.12 (d, *J* = 8.1 Hz, 1H), 7.95 (d, *J* = 8.3 Hz, 1H), 7.84 – 7.71 (m, 4H), 7.56 (dd, *J* = 8.5, 1.6 Hz, 2H), 7.45 (dd, *J* = 8.2, 1.5 Hz, 1H), 7.36 (dd, *J*

= 8.3, 1.6 Hz, 1H), 4.27 (t, *J* = 7.2 Hz, 2H), 1.94 (h, *J* = 7.4 Hz, 2H), 1.01 (t, *J* = 7.4 Hz, 3H). ^{13}C NMR (101 MHz, $CDCl_3$) δ 146.29, 140.93, 139.70, 132.64, 132.59, 130.45, 128.89, 127.61, 125.65, 124.47, 123.24, 122.51, 119.32, 119.22, 112.14, 110.57, 109.97, 109.62, 77.37, 77.05, 76.73, 44.94, 22.32, 11.78.

Synthesis of 4-(6-(3-(1-phenyl-1*H*-phenanthro[9,10-*d*]imidazol-2-yl)phenyl)-9-propyl-9*H*-carbazol-3-yl)benzonitrile (3,6-mPPICNC3): Under nitrogen atmosphere, **3-CNC3** (1.1 g, 2.7 mmol), 1-phenyl-2-(3-(4,4,5,5-tetramethyl-1,3,2-dioxaborolan-2-yl)phenyl)-1*H*-phenanthro[9,10-*d*]imidazole (1.4 g, 2.9 mmol) and $Pd(PPh_3)_4$ (0.2 g, 0.2 mmol) were placed in a 250 mL two-neck round-bottom flask. Then, THF (60 mL), 2 M potassium carbonate (10.0 mL) were injected. The reaction mixture was stirred and refluxed at 80 ℃ for 24 h. After cooling to room temperature, the reaction mixture was extracted 3 times with CH_2Cl_2 and water. The organic layer was dried with anhydrous $MgSO_4$, filtered, and evaporated under reduced pressure. The crude product was purified by silica-gel column chromatography using petroleum / CH_2Cl_2 (4/1, v/v) as the eluting agent. Finally further purified by a multi-temperature-zone sublimator, a white solid was obtained (1.6 g, 89%). ^{1}H NMR (400 MHz, $CDCl_3$) δ 8.80 (d, J = 8.4 Hz, 1H), 8.73 (d, J = 8.3 Hz, 1H), 8.40 (d, J = 1.8 Hz, 1H), 8.19 (s, 1H), 7.97 (s, 1H), 7.88 – 7.81 (m, 2H), 7.80 – 7.67 (m, 8H), 7.65 – 7.39 (m, 8H), 7.32 – 7.26 (m, 3H), 7.22 (d, J = 8.2 Hz, 1H), 4.34 (t, J = 7.1 Hz, 2H), 1.98 (h, J = 7.3 Hz, 2H), 1.02 (t, J = 7.4 Hz, 3H). ^{13}C NMR (101 MHz, $CDCl_3$) δ 146.64, 141.15, 140.70, 132.69, 130.45, 130.20, 129.27, 128.90, 127.79, 127.60, 125.74, 125.17, 124.25, 123.72, 123.29, 123.15, 120.97, 119.34, 119.18, 109.85, 109.53, 109.36, 44.96, 22.42, 11.84. TOF-MS(ESI) m/z calcd. for $C_{49}H_{34}N_4$: 678.2783; $[M+H]^+$ found: 679.2866.

Synthesis of 4-(6-(4-(1-phenyl-1*H*-phenanthro[9,10-*d*]imidazol-2-yl)phenyl)-9-propyl-9*H*-carbazol-3-yl)benzonitrile (3,6-pPPICNC3): The synthetic procedure of **3,6-pPPICNC3** is

similar to that of **3,6-mPPICNC3** with **3-CNC3** (1.0 g, 2.5 mmol), 1-phenyl-2-(4-(4,4,5,5-tetramethyl-1,3,2-dioxaborolan-2-yl)phenyl)-1*H*-phenanthro[9,10-*d*]imidazole (1.3 g, 2.6 mmol) and $Pd(PPh_3)_4$ (0.2 g, 0.2 mmol) as starting materials, giving a white solid (1.2 g, 70%).^{1}H NMR (400 MHz, $CDCl_3$) δ 9.00 (s, 1H), 8.79 (d, J = 8.4 Hz, 1H), 8.72 (d, J = 8.3 Hz, 1H), 8.36 (t, J = 2.2 Hz, 2H), 7.87 – 7.63 (m, 15H), 7.62 – 7.56 (m, 2H), 7.56 – 7.46 (m, 3H), 7.31 – 7.26 (m, 1H), 7.19 (d, J = 8.2 Hz, 1H), 4.32 (t, J = 7.1 Hz, 2H), 1.96 (p, J = 7.3 Hz, 2H), 1.01 (t, J = 7.4 Hz, 3H). ^{13}C NMR (101 MHz, $CDCl_3$) δ 146.49, 141.16, 140.80, 132.63, 130.35, 130.24, 129.96, 129.18, 127.62, 126.91, 126.41, 125.58, 125.20, 124.18, 123.65, 123.33, 123.13, 120.91, 119.26, 118.93, 109.85, 109.55, 109.43, 44.96, 22.40, 11.83. TOF-MS(ESI) m/z calcd. for $C_{49}H_{34}N_4$: 678.2783; $[M+H]^+$ found: 679.2866.

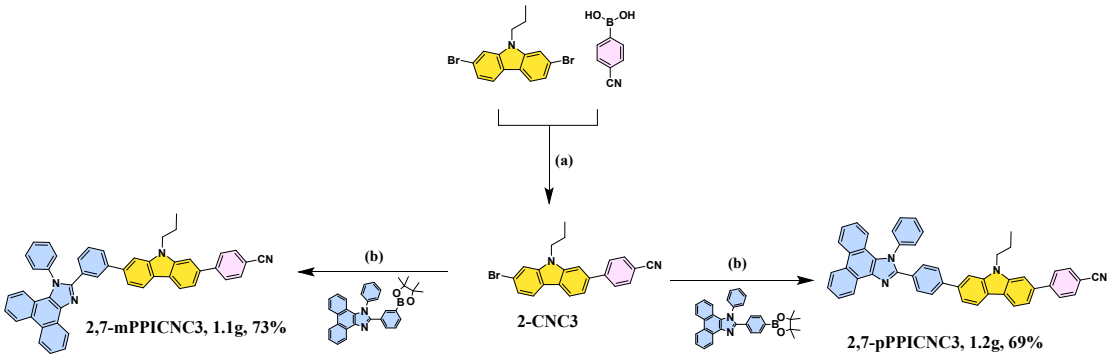

Scheme 3. Synthetic routes to **2,7-mPPICNC3** and **2,7-pPPICNC3**. (a) $Pd(PPh_3)_4$, K_2CO_3 (2M), THF, 75 ℃, 18 h. (b) $Pd(PPh_3)_4$, K_2CO_3 (2M), THF, 80 ℃, 24 h.

Synthesis of 4-(7-bromo-9-propyl-9*H*-carbazol-2-yl)benzonitrile (2-CNC3): The synthetic procedure of **2-CNC3** is similar to that of **3-NC3** with **2,7-Br-C3Cz** (13.2 g, 36.1 mmol), (4-cyanophenyl)boronic acid (2.5 g, 17.2 mmol) and $Pd(PPh_3)_4$ (0.7 g, 0.6 mmol) as the starting materials, giving a white solid (3.2 g, 48%).^{1}H NMR (400 MHz, $CDCl_3$) δ 8.26 (t, *J* = 2.0 Hz, 2H), 7.83 – 7.67 (m, 5H), 7.57 (dd, *J* = 8.7, 1.9 Hz, 1H), 7.49 (d, *J* = 8.6 Hz, 1H), 7.32 (d, *J* = 8.7 Hz, 1H), 4.29 (t, *J* = 7.1 Hz, 2H), 1.93 (h, *J* = 7.3 Hz, 2H), 0.98 (t, *J* = 7.4 Hz, 3H). ^{13}C NMR (101 MHz, $CDCl_3$) δ 146.52, 142.03, 141.10, 137.31, 132.63, 128.15, 122.68, 122.48,

121.75, 121.29, 120.96, 119.96, 119.07, 118.92, 112.06, 110.71, 107.62, 77.38, 77.06, 76.74, 44.83, 22.29, 11.82.

Synthesis of 4-(7-(3-(1-phenyl-1*H*-phenanthro[9,10-*d*]imidazol-2-yl)phenyl)-9-propyl-9*H*-carbazol-2-yl)benzonitrile (2,7-mPPICNC3): The synthetic procedure of **2,7-mPPICNC3** is similar to that of **3,6-mPPICNC3** with **2-CNC3** (1.0 g, 2.6 mmol), 1-phenyl-2-(4-(4,4,5,5-tetramethyl-1,3,2-dioxaborolan-2-yl)phenyl)-1*H*-phenanthro[9,10-*d*]imidazole (1.3 g, 2.6 mmol) and $Pd(PPh_3)_4$ (0.2 g, 0.2 mmol) as the starting materials, giving a white solid powder (1.2 g, 69%). ^{1}H NMR (400 MHz, $CDCl_3$) δ 8.93 (s, 1H), 8.79 (d, J = 8.3 Hz, 1H), 8.73 (d, J = 8.3 Hz, 1H), 8.16 (dd, J = 10.3, 8.0 Hz, 2H), 7.85 – 7.80 (m, 2H), 7.79 – 7.70 (m, 5H), 7.69 – 7.64 (m, 5H), 7.63 – 7.57 (m, 4H), 7.55 – 7.45 (m, 3H), 7.31 – 7.26 (m, 2H), 7.20 (dd, J = 8.4, 1.4 Hz, 1H), 4.38 (t, J = 7.2 Hz, 2H), 2.00 (p, J = 7.3 Hz, 2H), 1.04 (t, J = 7.4 Hz, 3H). ^{13}C NMR (101 MHz, $CDCl_3$) δ 144.17, 142.15, 141.67, 141.59, 140.98, 138.67, 138.26, 138.01, 130.31, 129.92, 129.44, 129.30, 128.80, 128.41, 128.28, 128.11, 127.47, 126.67, 126.39, 126.17, 126.05, 125.87, 125.67, 125.12, 124.20, 123.44, 123.18, 123.02, 122.92, 122.34, 121.94, 120.94, 120.85, 120.66, 120.41, 120.03, 118.91, 118.68, 109.94, 107.42, 107.37, 44.65, 22.44, 11.92. TOF-MS(ESI) m/z calcd. for $C_{49}H_{34}N_4$: 678.2783; $[M+H]^+$ found: 679.2862.

Synthesis of 4-(7-(3-(1-phenyl-1*H*-phenanthro[9,10-*d*]imidazol-2-yl)phenyl)-9-propyl-9*H*-carbazol-2-yl)benzonitrile (2,7-pPPICNC3): The synthetic procedure of **2,7-pPPICNC3** is similar to that of **3,6-mPPICNC3** with **2-CNC3** (0.9 g, 2.6 mmol), 1-phenyl-2-(3-(4,4,5,5-tetramethyl-1,3,2-dioxaborolan-2-yl)phenyl)-1*H*-phenanthro[9,10-*d*]imidazole (1.2 g, 2.4 mmol) and $Pd(PPh_3)_4$ (0.2 g, 0.2 mmol) as the starting materials, giving as a light yellow solid powder (1.1 g, 73%). ^{1}H NMR (400 MHz, $CDCl_3$) δ 8.94 (s, 1H), 8.76 (ddd, J = 25.3, 8.4, 1.1 Hz, 2H), 8.14 (dd, J = 19.5, 8.1 Hz, 2H), 7.96 (s, 1H), 7.84 – 7.75 (m, 5H), 7.68 (dh, J = 7.9, 1.8 Hz, 5H), 7.61 (dd, J = 2.4, 1.3 Hz, 2H), 7.58 (d, J = 1.5 Hz, 1H), 7.56 – 7.40 (m, 4H), 7.35

– 7.14 (m, 4H), 4.39 (t, J = 7.1 Hz, 2H), 2.00 (q, J = 7.3 Hz, 2H), 1.04 (t, J = 7.4 Hz, 3H). ^{13}C NMR (101 MHz, DMSO-*d*) δ 150.43, 146.14, 142.03, 141.81, 141.78, 139.02, 137.83, 137.31, 136.46, 132.92, 130.79, 130.55, 129.65, 129.52, 129.50, 129.11, 128.40, 128.27, 127.49, 127.32, 127.07, 126.67, 125.89, 125.33, 124.71, 123.82, 123.04, 122.73, 122.46, 121.88, 121.21, 120.65, 119.15, 118.41, 118.39, 110.18, 108.25, 107.74, 44.00, 22.37, 11.46. TOF-MS(ESI) m/z calcd. for $C_{49}H_{34}N_4$: 678.2783; $[M+H]^+$ found: 679.2864.

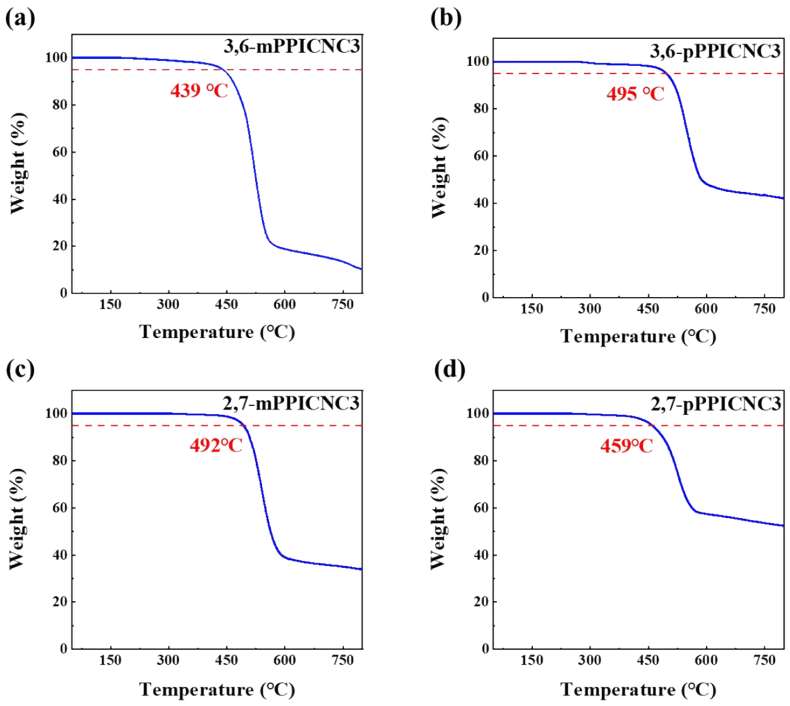

Figure S1. TGA thermograms of **3,6-mPPICNC3**, **3,6-pPPICNC3**, **2,7-mPPICNC3** and **2,7-pPPICNC3**.

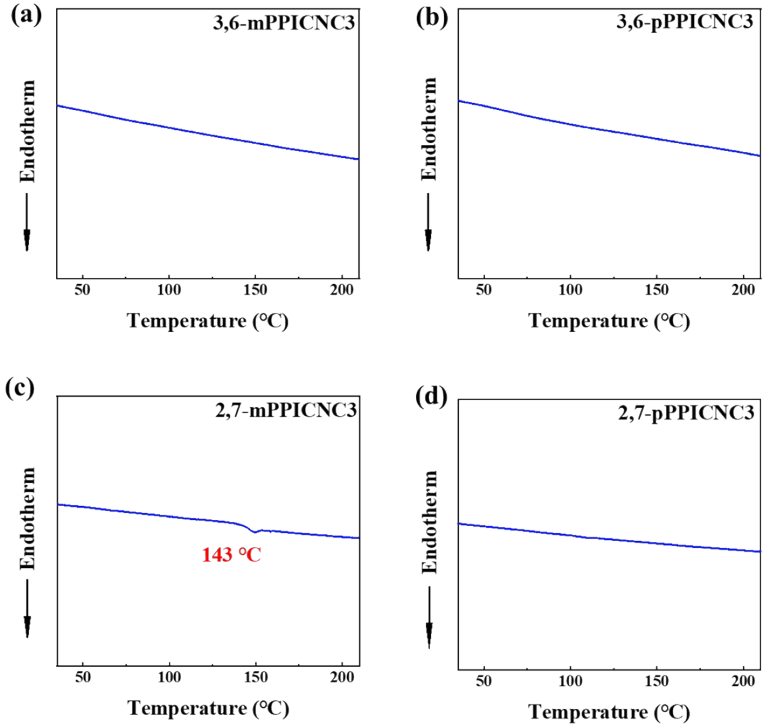

Figure S2. DSC curves of **3,6-mPPICNC3**, **3,6-pPPICNC3**, **2,7-mPPICNC3** and **2,7-pPPICNC3**.

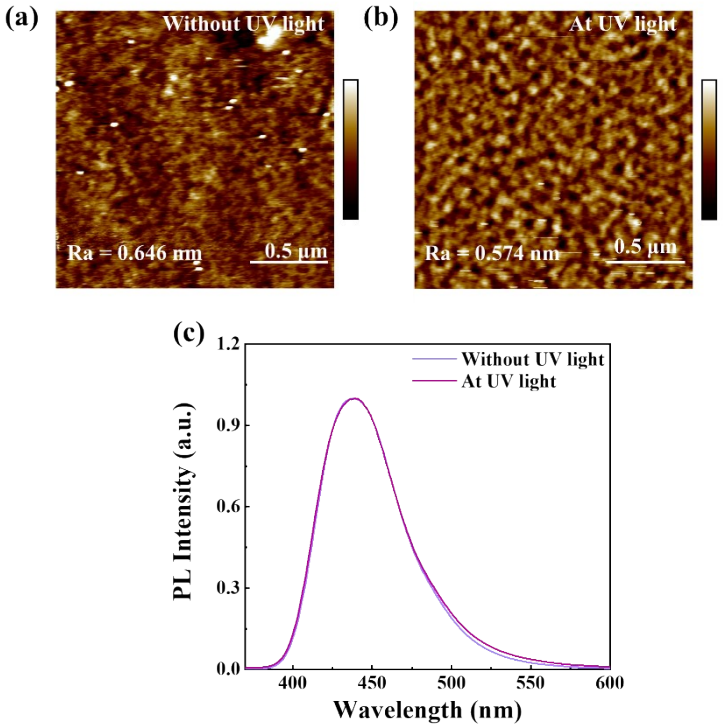

Figure S3. (a) and (b) Atomic Force Microscope (AFM) height images of **3,6-pPPICNC3** films without/with exposure at ultraviolet lamp. (c) PL spectra of **3,6-pPPICNC3** films without/with exposure at ultraviolet lamp

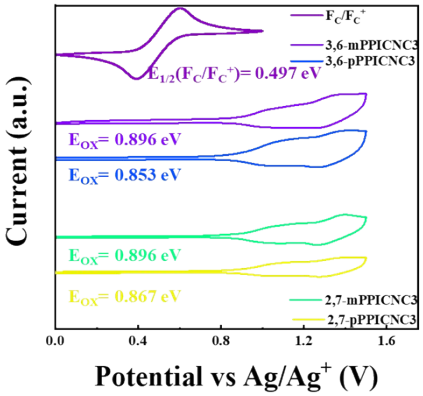

Figure S4. Cyclic voltammograms in dichloromethane solution of **3,6-mPPICNC3**, **3,6-pPPICNC3**, **2,7-mPPICNC3** and **2,7-pPPICNC3**.

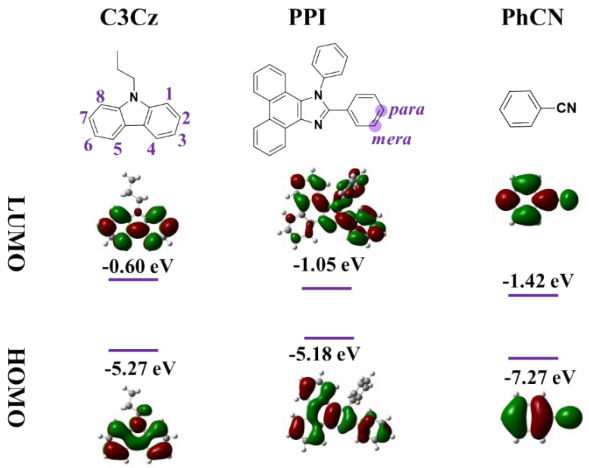

Figure S5. Frontier molecular orbitals (FMOs) and chemical structures of *N*-propyl-modified carbazole (C3Cz), benzonitrile (PhCN) and 1,2-diphenyl-1*H*-phenanthro[9,10-*d*]imidazole (PPI).

Table S1. Bond length in S_0 and S_1 of **3,6-mPPICNC3, 3,6-pPPICNC3, 2,7-mPPICNC3** and **2,7-pPPICNC3**.

Compounds	Structure	S_0			S_1		
		L_1 [Å]	L_2 [Å]	L_3 [Å]	L_1 [Å]	L_2 [Å]	L_3 [Å]
3,6-mPPICNC3	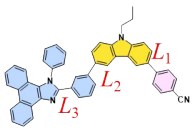	1.477	1.481	1.467	1.455	1.476	1.450
3,6-pPPICNC3	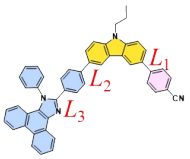	1.478	1.479	1.467	1.455	1.452	1.439
2,7-mPPICNC3	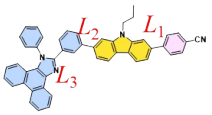	1.479	1.481	1.470	1.448	1.470	1.451
2,7-pPPICNC3	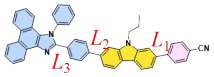	1.479	1.479	1.467	1.456	1.450	1.437

Table S2. NTOs analysis of singlet and triplet excited states for **3,6-mPPICNC3**.

3,6-mPPICNC3								
Singlets					**Triplets**			
	Hole			Particle		Hole		Particle
$S_0 \rightarrow S_1$	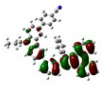	**99.80%**	→	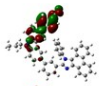	$S_0 \rightarrow T_1$	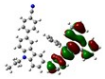	**75.16%**	→ 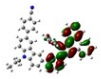
$S_0 \rightarrow S_2$		**93.43%**	→	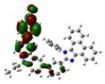	$S_0 \rightarrow T_2$	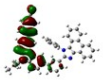	**77.16%**	→ 
$S_0 \rightarrow S_3$	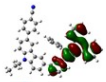	**93.43%**	→	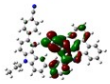	$S_0 \rightarrow T_3$	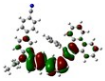	**63.75%**	→ 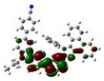
$S_0 \rightarrow S_4$	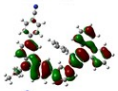	**85.41%**	→	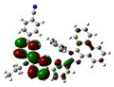	$S_0 \rightarrow T_4$	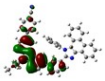	**74.70%**	→ 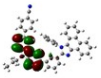
$S_0 \rightarrow S_5$	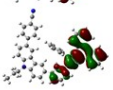	**74.99%**	→	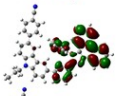	$S_0 \rightarrow T_5$	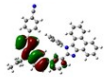	**56.59%**	→ 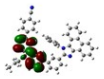
$S_0 \rightarrow S_6$	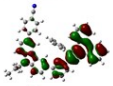	**82.61%**	→	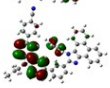	$S_0 \rightarrow T_6$	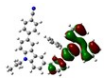	**91.82%**	→ 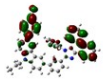
$S_0 \rightarrow S_7$	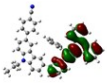	**84.48%**	→	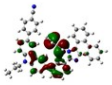	$S_0 \rightarrow T_7$	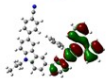	**87.71%**	→ 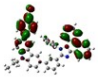
$S_0 \rightarrow S_8$	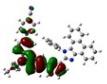	**78.96%**	→	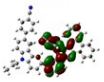	$S_0 \rightarrow T_8$	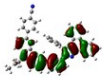	**68.69%**	→ 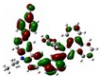
$S_0 \rightarrow S_9$	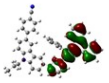	**63.52%**	→	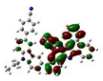	$S_0 \rightarrow T_9$	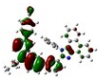	**54.35%**	→ 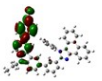
$S_0 \rightarrow S_{10}$	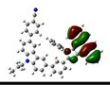	**92.87%**	→	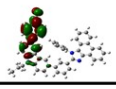	$S_0 \rightarrow T_{10}$	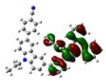	**72.30%**	→ 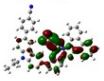

Table S3. NTOs analysis of singlet and triplet excited states for **2,7-mPPICNC3**.

2,7-mPPICNC3							
Singlets				**Triplets**			
	Hole		Particle		Hole		Particle
$S_0 \rightarrow S_1$	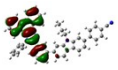	**99.25%**	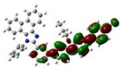	$S_0 \rightarrow T_1$	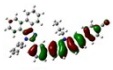	**60.27%**	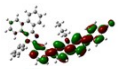
$S_0 \rightarrow S_2$	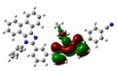	**96.90%**	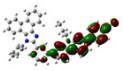	$S_0 \rightarrow T_2$	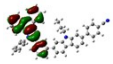	**51.98%**	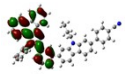
$S_0 \rightarrow S_3$	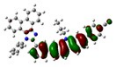	**80.59%**	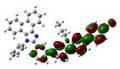	$S_0 \rightarrow T_3$	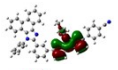	**96.17%**	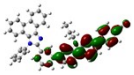
$S_0 \rightarrow S_4$	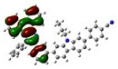	**77.44%**	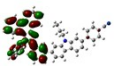	$S_0 \rightarrow T_4$	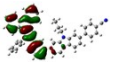	**67.62%**	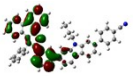
$S_0 \rightarrow S_5$	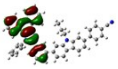	**92.38%**	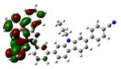	$S_0 \rightarrow T_5$	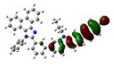	**67.15%**	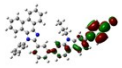
$S_0 \rightarrow S_6$	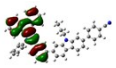	**75.18%**	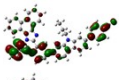	$S_0 \rightarrow T_6$	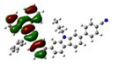	**96.19%**	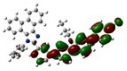
$S_0 \rightarrow S_7$	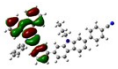	**88.17%**	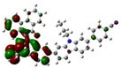	$S_0 \rightarrow T_7$	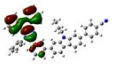	**90.40%**	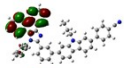
$S_0 \rightarrow S_8$	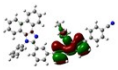	**92.38%**	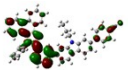	$S_0 \rightarrow T_8$	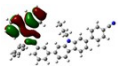	**77.67%**	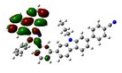
$S_0 \rightarrow S_9$	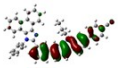	**73.56%**	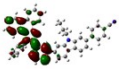	$S_0 \rightarrow T_9$	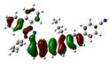	**68.46%**	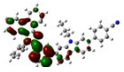
$S_0 \rightarrow S_{10}$	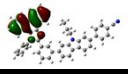	**94.03%**	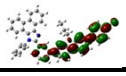	$S_0 \rightarrow T_{10}$	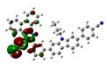	**62.35%**	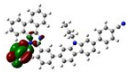

Table S4. NTOs analysis of singlet and triplet excited states for **3,6-pPPICNC3**.

3,6-pPPICNC3							
Singlets				**Triplets**			
	Hole		Particle		Hole		Particle
$S_0 \rightarrow S_1$	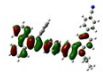	**98.95%**		$S_0 \rightarrow T_1$		**82.36%**	
$S_0 \rightarrow S_2$	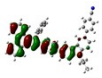	**97.32%**		$S_0 \rightarrow T_2$		**71.97%**	
$S_0 \rightarrow S_3$	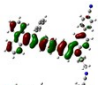	**84.58%**		$S_0 \rightarrow T_3$		**61.72%**	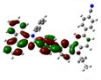
$S_0 \rightarrow S_4$	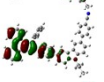	**90.01%**		$S_0 \rightarrow T_4$		**85.48%**	
$S_0 \rightarrow S_5$	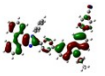	**87.03%**		$S_0 \rightarrow T_5$		**57.95%**	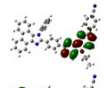
$S_0 \rightarrow S_6$	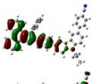	**93.35%**		$S_0 \rightarrow T_6$	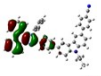	**91.23%**	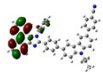
$S_0 \rightarrow S_7$	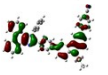	**67.90%**		$S_0 \rightarrow T_7$		**89.65%**	
$S_0 \rightarrow S_8$	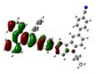	**77.59%**		$S_0 \rightarrow T_8$		**64.00%**	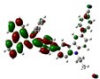
$S_0 \rightarrow S_9$	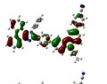	**79.23%**		$S_0 \rightarrow T_9$		**69.31%**	
$S_0 \rightarrow S_{10}$	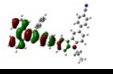	**57.22%**		$S_0 \rightarrow T_{10}$	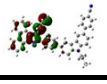	**64.36%**	

Table S5. NTOs analysis of singlet and triplet excited states for **2,7-pPPICNC3**.

2,7-pPPICNC3							
Singlets				**Triplets**			
	Hole		Particle		Hole		Particle
$S_0 \rightarrow S_1$	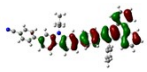	**99.14%**	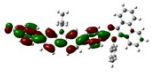	$S_0 \rightarrow T_1$	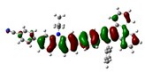	**79.77%**	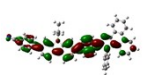
$S_0 \rightarrow S_2$	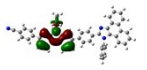	**96.22%**	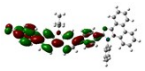	$S_0 \rightarrow T_2$	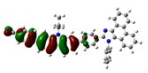	**84.32%**	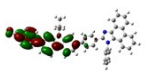
$S_0 \rightarrow S_3$	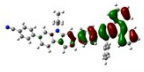	**85.15%**	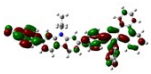	$S_0 \rightarrow T_3$	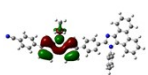	**92.16%**	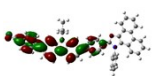
$S_0 \rightarrow S_4$		**80.01%**	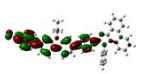	$S_0 \rightarrow T_4$	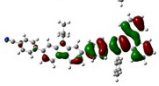	**64.69%**	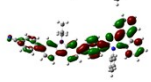
$S_0 \rightarrow S_5$	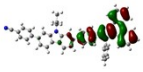	**87.21%**	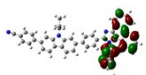	$S_0 \rightarrow T_5$	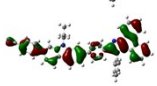	**79.35%**	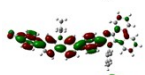
$S_0 \rightarrow S_6$	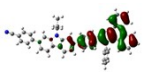	**84.08%**	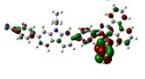	$S_0 \rightarrow T_6$	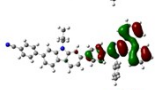	**91.41%**	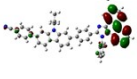
$S_0 \rightarrow S_7$	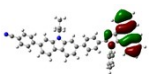	**61.21%**	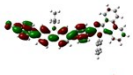	$S_0 \rightarrow T_7$	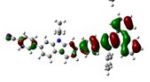	**83.13%**	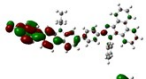
$S_0 \rightarrow S_8$	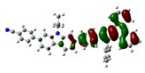	**76.08%**	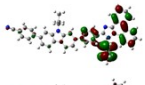	$S_0 \rightarrow T_8$	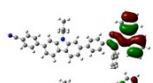	**76.32%**	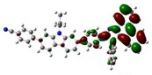
$S_0 \rightarrow S_9$	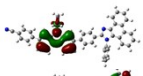	**95.16%**	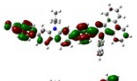	$S_0 \rightarrow T_9$	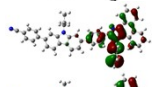	**59.01%**	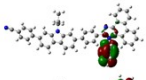
$S_0 \rightarrow S_{10}$	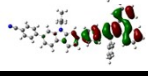	**70.72%**	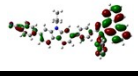	$S_0 \rightarrow T_{10}$	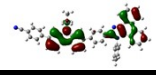	**65.33%**	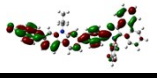

Table S6. Energy levels of singlet and triplet states, oscillator strengths of singlet states for **3,6-mPPICNC3** and **3,6-pPPICNC3**.

3,6-mPPICNC3					3,6-pPPICNC3				
S Excited States	**[eV]**	**T Excited States**	**[eV]**	**S Oscillator Strength**	**S Excited States**	**[eV]**	**T Excited States**	**[eV]**	**S Oscillator Strength**
S_1	3.343	T_1	2.710	0.0321	S_1	3.285	T_1	2.606	0.4862
S_2	3.489	T_2	2.826	0.1934	S_2	3.491	T_2	2.840	0.6983
S_3	3.597	T_3	3.042	0.0770	S_3	3.608	T_3	2.973	0.0482
S_4	3.648	T_4	3.170	0.6468	S_4	3.677	T_4	3.150	0.0151
S_5	3.736	T_5	3.228	0.0156	S_5	3.698	T_5	3.234	0.2772
S_6	3.765	T_6	3.339	0.3918	S_6	3.840	T_6	3.319	0.0888
S_7	3.908	T_7	3.354	0.0169	S_7	3.896	T_7	3.367	0.0424
S_8	3.914	T_8	3.440	0.0396	S_8	3.904	T_8	3.460	0.0447
S_9	3.941	T_9	3.548	0.0894	S_9	4.003	T_9	3.593	0.0117
S_{10}	3.988	T_{10}	3.614	0.0280	S_{10}	4.050	T_{10}	3.666	0.0122

Table S7. Energy levels of singlet and triplet states, oscillator strengths of singlet states for **2,7-mPPICNC3** and **2,7-pPPICNC3**.

2,7-mPPICNC3					2,7-pPPICNC3				
S Excited States	**[eV]**	**T Excited States**	**[eV]**	**S Oscillator Strength**	**S Excited States**	**[eV]**	**T Excited States**	**[eV]**	**S Oscillator Strength**
S_1	3.343	T_1	2.626	0.0284	S_1	3.107	T_1	2.506	1.0726
S_2	3.390	T_2	2.716	0.0196	S_2	3.384	T_2	2.732	0.0173
S_3	3.513	T_3	2.936	1.2908	S_3	3.560	T_3	2.934	0.7868
S_4	3.695	T_4	3.065	0.2582	S_4	3.658	T_4	3.279	0.2949
S_5	3.741	T_5	3.253	0.0148	S_5	3.689	T_5	3.326	0.0368
S_6	3.912	T_6	3.324	0.0005	S_6	3.848	T_6	3.333	0.0525
S_7	3.926	T_7	3.341	0.1000	S_7	3.860	T_7	3.518	0.0042
S_8	3.969	T_8	3.545	0.0347	S_8	3.940	T_8	3.767	0.0076
S_9	4.000	T_9	3.653	0.0053	S_9	3.961	T_9	3.804	0.0571
S_{10}	4.035	T_{10}	3.696	0.0008	S_{10}	4.076	T_{10}	3.845	0.0075

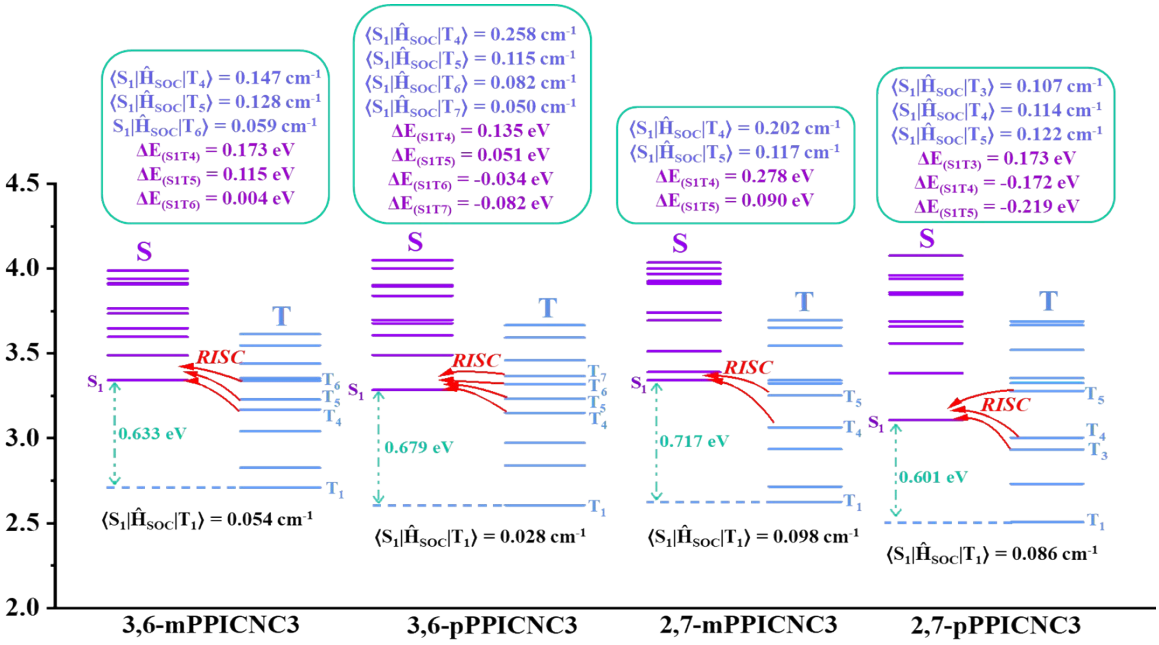

Figure S6. Singlet and triplet energy levels and SOC matrix elements of **3,6-mPPICNC3, 3,6-pPPICNC3, 2,7-mPPICNC3** and **2,7-pPPICNC3**, calculated by TD-DFT methods.

Detailed Analysis of High-lying RISC Process

As for **3,6-pPPICNC3**, The S_1/T_1 energy splitting (ΔE_{S1T1}) is as large as 0.633 eV with a small spin-orbit coupling (SOC) constant of 0.028 cm^{-1}, which is hardly to facilitate the upconversion of the excitions on T_1 to S_1 through the RISC process. The S_1 state of **3,6-pPPICNC3** shows a typical HLCT state characteristic, while the high-lying triplet states (T_4, T_5, T_6 and T_7) exhibit HLCT, LE, HLCT and CT- dominated HLCT states with small energy differences (0.135, 0.051, -0.034 and -0.082 eV) between S_1 and them. As Fermi's golden rule remarks, the RISC rate (k_{RISC}) has a close relationship with the SOC value and the energy gap between singlet and triplet states. The relationship can be expressed:

$$k_{RISC} \propto \left|\langle S|\hat{H}_{SOC}|T\rangle\right|^2 exp\left(\frac{-\Delta E_{ST}}{k_B T_r}\right) \quad (1)$$

Here, k_B is the Boltzmann constant, $\langle S|\hat{H}_{SOC}|T\rangle$ is the SOC matrix element between singlet and triplet states, and T_r is temperature. The SOC values between S_1 and T_4, T_5, T_6 and T_7 for **3,6-pPPICNC3** are as large as 0.258, 0.115, 0.082 and 0.050 cm^{-1}, which facilitate multichannel high-lying RISC processes from T_4, T_5, T_6 and T_7 to S_1.

As for **2,7-mPPICNC3** and **2,7-pPPICNC3** with the CT- dominated HLCT and HLCT state features, the ΔE_{S1T1} values are 0.717 and 0.601 eV with SOC constants of 0.098 and 0.086 cm^{-1}, which illustrates the thermally activated delayed fluorescence mechanism can be excluded. Both T_4 and T_5 states for **2,7-mPPICNC3** exhibit obvious LE states with small energy differences of 0.278 and 0.090 eV and large SOC values of 0.202 and 0.117 cm^{-1} between S_1 and them, while all the T_3, T_4 and T_5 states for **2,7-pPPICNC3** show obvious HLCT states with small energy differences of 0.173, -0.172 and -0.219 eV and large SOC values of 0.107, 0.114 and 0.122 cm^{-1} between S_1 and them. This could facilitate thehigh-lying RISC processes from T_4 and T_5 to S_1 for **2,7-mPPICNC3**, and from T_3, T_4 and T_5 to S_1 for **2,7-pPPICNC3**.

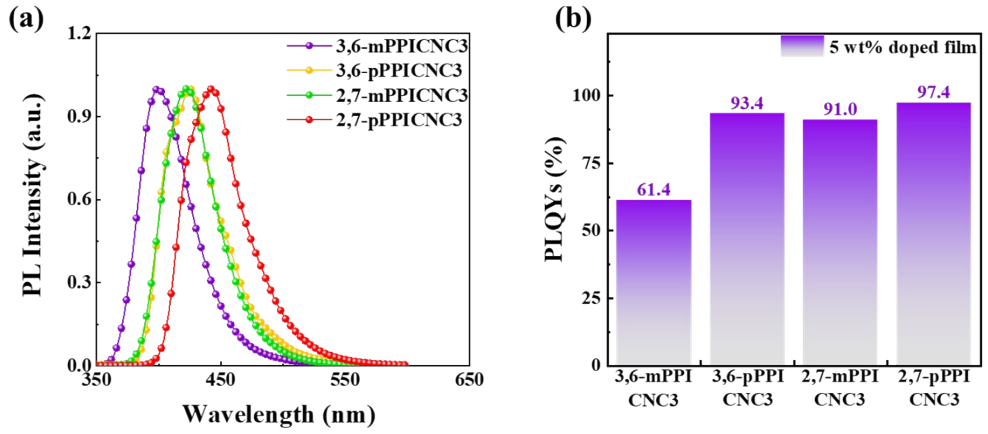

Figure S7. (a) Normalized PL spectra of 5 wt% doped in PMMA films and (b) PLQYs in 5 wt% doped in PMMA films of **3,6-mPPICNC3, 3,6-pPPICNC3, 2,7-mPPICNC3** and **2,7-pPPICNC3**.

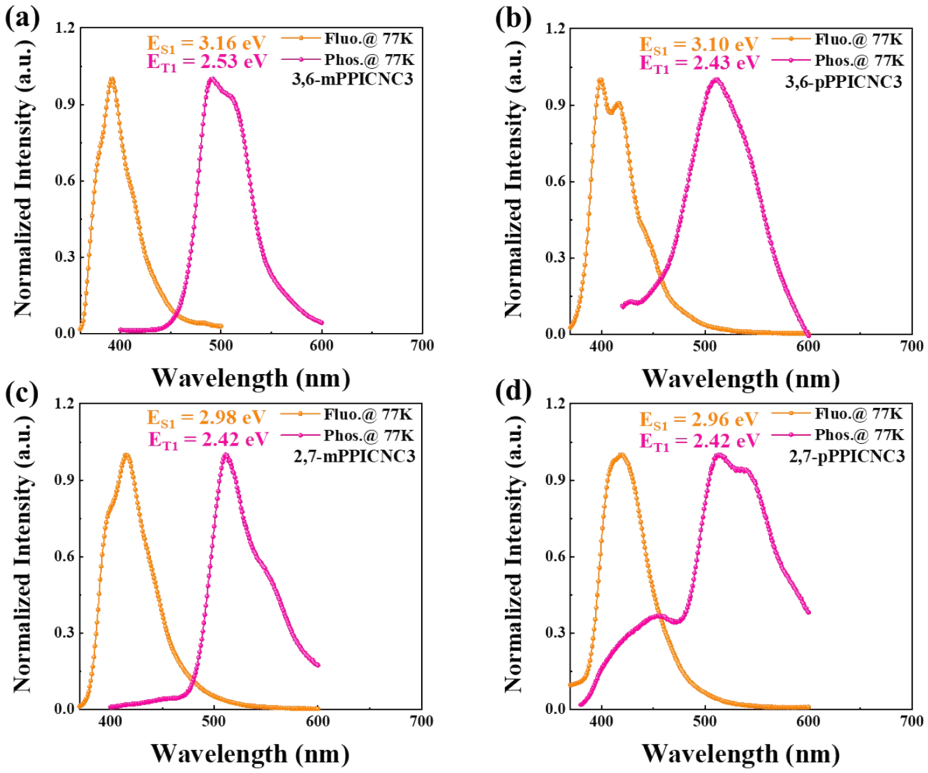

Figure S8. Low-temperature fluorescence and phosphorescence spectra of **3,6-mPPICNC3** (a), **3,6-pPPICNC3** (b), **2,7-mPPICNC3** (c), and **2,7-pPPICNC3** (d) in toluene solution (10^{-5} M) at 77 K.

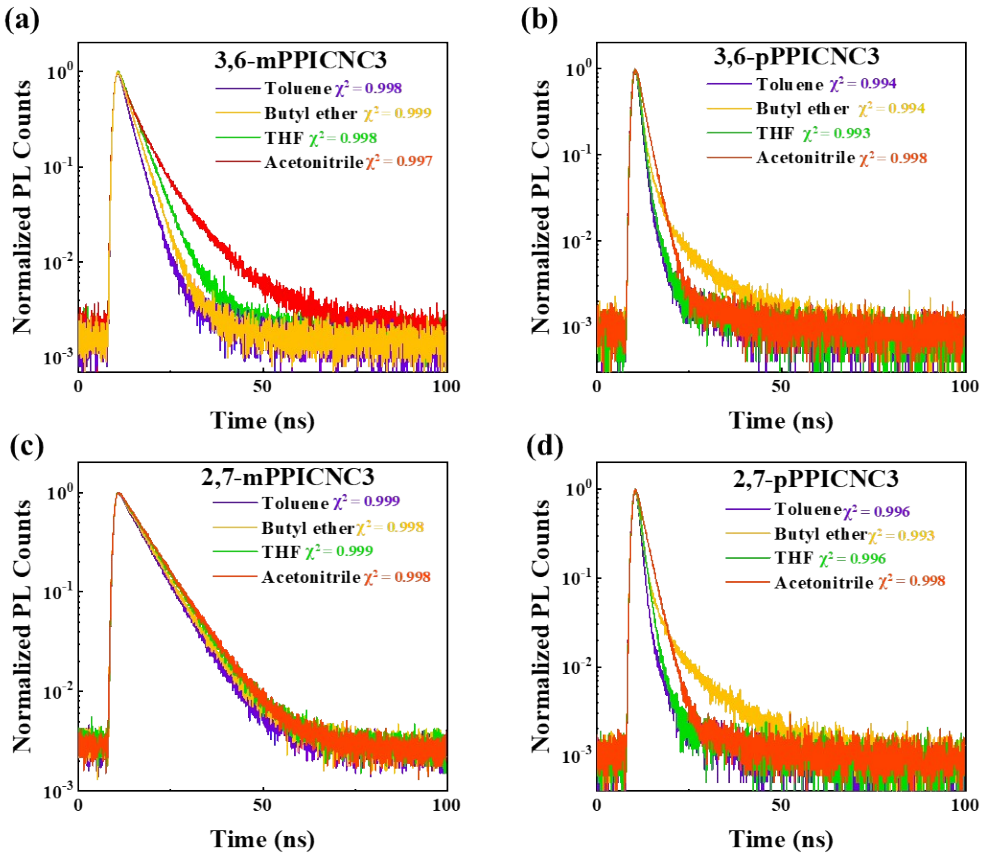

Figure S9. Transient PL decay spectra at toluene, butyl ether, THF, and acetonitrile solutions (10^{-5} M) of (a) **3,6-mPPICNC3**, (b) **3,6-pPPICNC3**, (c) **2,7-mPPICNC3** and (d) **2,7-pPPICNC3**. All the curves fitted by single-exponential decays with the χ^2 values exceeding 0.993.

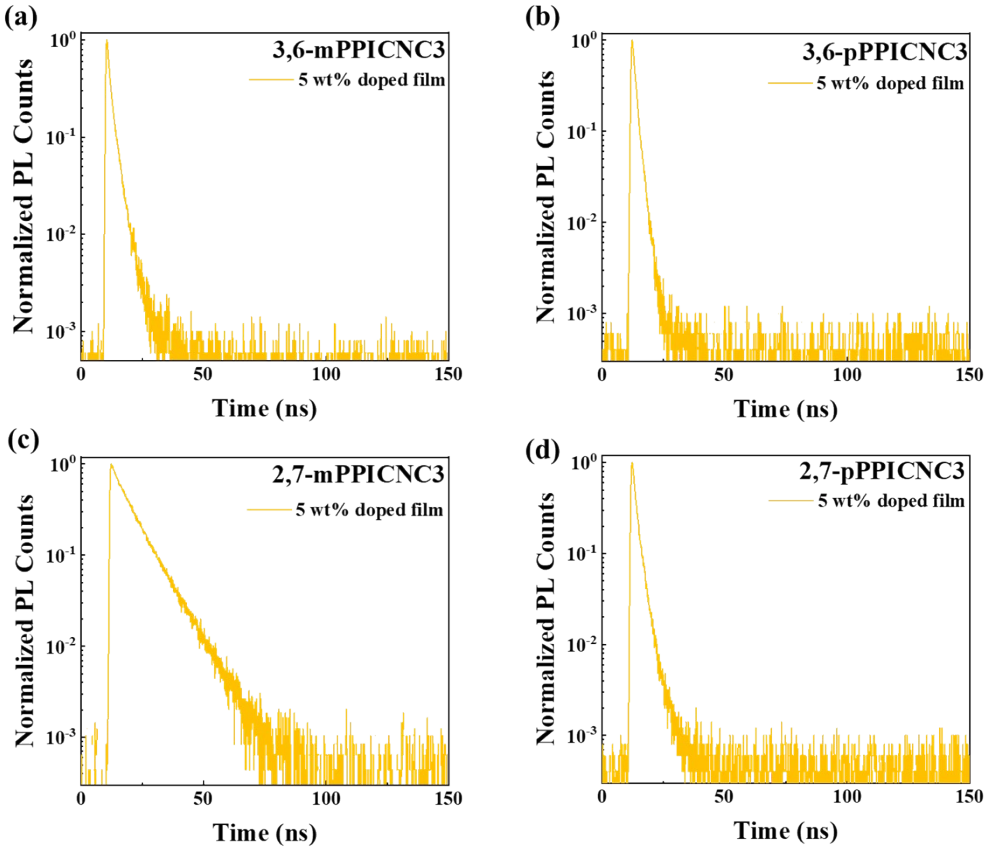

Figure S10. Transient PL decay spectra at 5 wt% doped films of (a) **3,6-mPPICNC3**, (b) **3,6-pPPICNC3**, (c) **2,7-mPPICNC3** and (d) **2,7-pPPICNC3**.

Table S8. PLQYs (Φ_{PL}s), fluorescence lifetime (τ), radiative transition rate (k_r) and non-radiative transition rate (k_{nr}) of **3,6-mPPICNC3**, **3,6-pPPICNC3**, **2,7-mPPICNC3** and **2,7-pPPICNC3**.

	Φ_{PL} [%]	τ [ns]	k_r[a] [$\times 10^8$ s^{-1}]	k_{nr}[b] [$\times 10^8$ s^{-1}]	Φ_{PL} [%]	τ [ns]	k_r[a] [$\times 10^8$ s^{-1}]	k_{nr}[b] [$\times 10^8$ s^{-1}]
	3,6-mPPICNC3				**3,6-pPPICNC3**			
Toluene	82.6	3.01	2.74	0.58	95.3	1.29	7.39	0.36
Butyl ether	92.9	3.67	2.53	0.19	95.4	1.66	5.75	0.28
Tetrahydrofuran	94.3	4.37	2.16	0.13	96.2	1.31	7.34	0.29
Acetonitrile	97.8	4.96	1.97	0.04	96.8	2.20	4.40	0.15
5 wt% doped into PMMA	61.4	2.58	2.38	1.49	93.4	1.32	7.08	0.50
Neat film	59.1	1.55	3.81	2.64	63.0	1.33	4.74	2.77
	2,7-mPPICNC3				**2,7-pPPICNC3**			
Toluene	93.3	6.73	1.39	0.10	97.5	1.39	7.01	0.18
Butyl ether	93.6	6.82	1.37	0.09	97.9	1.54	6.36	0.14
Tetrahydrofuran	96.9	7.31	1.33	0.04	98.4	1.63	6.04	0.10
Acetonitrile	83.8	7.60	1.10	0.21	98.5	2.54	3.88	0.06
5 wt% doped into PMMA	91.0	7.88	1.15	0.11	97.4	1.63	5.98	0.16
Neat film	61.9	3.19	1.94	1.19	63.3	1.01	6.27	3.63

[a] $k_r = \Phi_{PL}/\tau$; [b] $k_{nr} = 1/\tau - k_r$

Detailed Analysis of Lippert-Mataga model

The Stokes shift ($\nu_a - \nu_f$) versus orientational polarizability ($f(\varepsilon, n)$) of solvents can be constructed by the Lippert-Mataga model with the Equation 1 as below.

$$hc(\nu_a - \nu_f) = hc\left(\nu_a^0 - \nu_f^0\right) + \frac{2(\mu_e - \mu_g)^2}{a_0^3} f(\varepsilon,n) \quad (1)$$

Here, h is the Plank constant, c is the light speed in vacuum, μ_g and μ_e are the ground-state excited-state dipole moments, $f(\varepsilon, n)$ is the orientational polarizability of solvents, a_0 is the Onsager cavity radius, $\nu_A^0 - \nu_f^0$ is the Stokes shifts when f is zero, respectively.

Take differential on both sides of the Equation 1, the Equation 2 can be obtained:

$$\mu_e = \mu_g + \{\frac{hca_0^3}{2} \times [\frac{d(\nu_A - \nu_f)}{df(\varepsilon, n)}]\}^{1/2} \quad (2)$$

(ε, n) and a_0 can be obtained by the Equation 3 and 4:

$$f(\varepsilon,n) = \frac{\varepsilon - 1}{2\varepsilon + 1} + \frac{n^2 - 1}{2n^2 + 1} \quad (3)$$

$$a_0 = (\frac{3M}{4\pi Nd})^{1/3} \quad (4)$$

Where, ε and n are dielectric constant and refractive index of solvent, N is Avogadro's number, M is molar mass, and d is density of the solvents, respectively. The values of $f(\varepsilon, n)$ and a_0 can be estimated by the Equation 3 and 4. The $\mu_g s$ of **3,6-mPPICNC3**, **3,6-pPPICNC3**, **2,7-mPPICNC3**, **2,7-pPPICNC3** were estimated to be 7.73, 4.77, 9.75 and 6.73 Debye by the Gaussian 09 package at the level of B3LYP/6-31G(d,p). The $\frac{d(\nu_A - \nu_f)}{df(\varepsilon, n)}$ can be estimated with the solvatochromic experiment data listed in Tables S8 and S9.

Table S9. The detailed absorption, emission peak and of **3,6-mPPICNC3** and **3,6-pPPICNC3** in different solvents.

Solvents	ε	n	$f(\varepsilon, n)$	3,6-mPPICNC3			3,6-pPPICNC3		
				λ_a [nm]	λ_f [nm]	$\nu_a - \nu_f$ [cm^{-1}]	λ_a [nm]	λ_f [nm]	$\nu_a - \nu_f$ [cm^{-1}]
Hexane	1.9	1.375	0.0012	326	367	3426.89	341	393	3880.22
Toluene	2.38	1.494	0.013	330	389	4596.09	343	400	4154.52
Triethylamine	2.42	1.401	0.048	328	387	4648.01	341	395	4009.06
Butyl ether	3.08	1.399	0.096	328	387	4648.01	341	396	4072.99
Isopropyl ether	3.88	1.368	0.145	327	387	4741.25	339	395	4182.07
Ethyl ether	4.34	1.352	0.167	326	387	4835.05	339	395	4182.07
Ethyl acetate	6.02	1.372	0.2	328	400	5487.80	340	398	4286.14
Tetrahydrofuran	7.58	1.407	0.21	330	403	5489.13	341	401	4387.86
Dichloromethane	8.93	1.424	0.217	330	414	6148.44	341	402	4449.89
Dimethylformamide	37	1.427	0.276	330	433	7208.34	344	407	4499.74
Acetone	20.7	1.359	0.284	330	422	6606.35	344	404	4317.29
Acetonitrile	37.5	1.344	0.305	330	432	7154.88	344	409	4619.89

Table S10. The detailed absorption and emission peaks of **2,7-mPPICNC3** and **2,7-pPPICNC3** in different solutions.

Solvents	ε	n	$f(\varepsilon, n)$	2,7-mPPICNC3			2,7-pPPICNC3		
				λ_a [nm]	λ_f [nm]	$\nu_a - \nu_f$ [cm^{-1}]	λ_a [nm]	λ_f [nm]	$\nu_a - \nu_f$ [cm^{-1}]
Hexane	1.9	1.375	0.0012	332	413	5907.41	367	409	2798.08
Toluene	2.38	1.494	0.013	335	424	6265.84	367	416	3209.49
Triethylamine	2.42	1.401	0.048	333	417	6049.21	367	412	2976.11
Butyl ether	3.08	1.399	0.096	332	418	6197.04	367	413	3034.88
Isopropyl ether	3.88	1.368	0.145	331	418	6288.04	365	411	3066.36
Ethyl ether	4.34	1.352	0.167	332	420	6310.96	364	411	3141.63
Ethyl acetate	6.02	1.372	0.2	333	426	6555.85	364	414	3317.94
Tetrahydrofuran	7.58	1.407	0.21	334	427	6520.92	364	417	3491.71
Dichloromethane	8.93	1.424	0.217	334	430	6684.31	366	419	3456.06
Dimethylformamide	37	1.427	0.276	337	439	6894.55	366	421	3569.44
Acetone	20.7	1.359	0.284	333	433	6935.34	365	422	3700.58
Acetonitrile	37.5	1.344	0.305	333	436	7094.25	363	423	3907.547

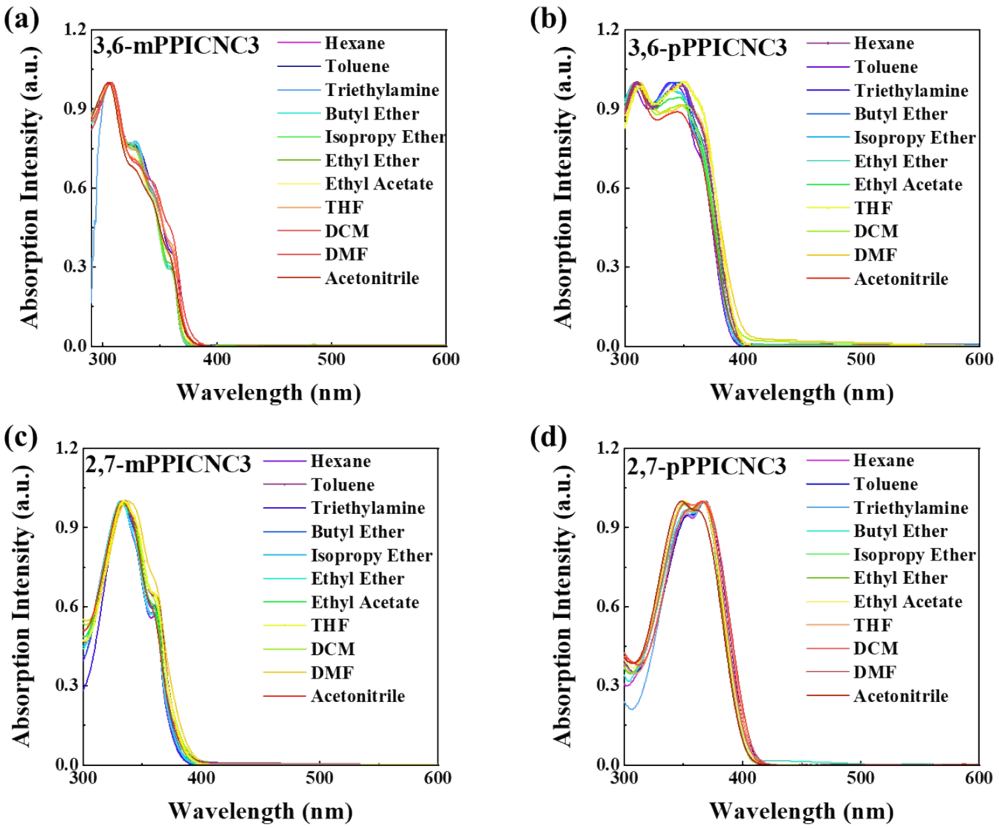

Figure S11. UV−vis absorption spectra of (a) **3,6-mPPICNC3**, (b) **3,6-pPPICNC3**, (c) **2,7-mPPICNC3** and (d) **2,7-pPPICNC3** in different solutions.

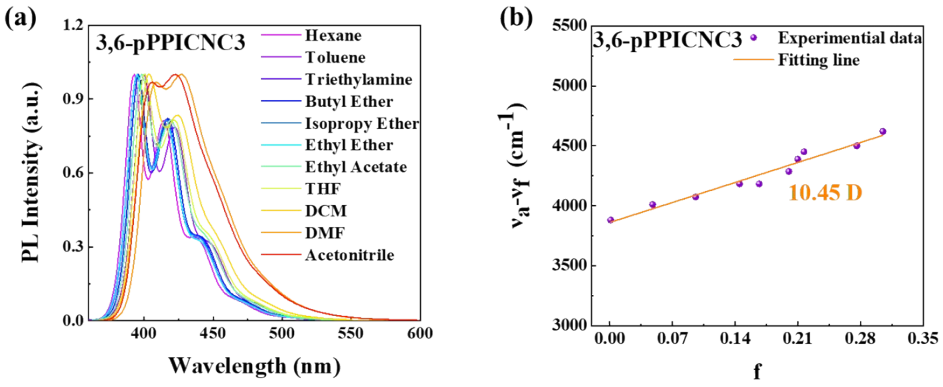

Figure S12. Solvation effects on PL spectra (a) and Lippert-Mataga plots (b) of **3,6-pPPICNC3**.

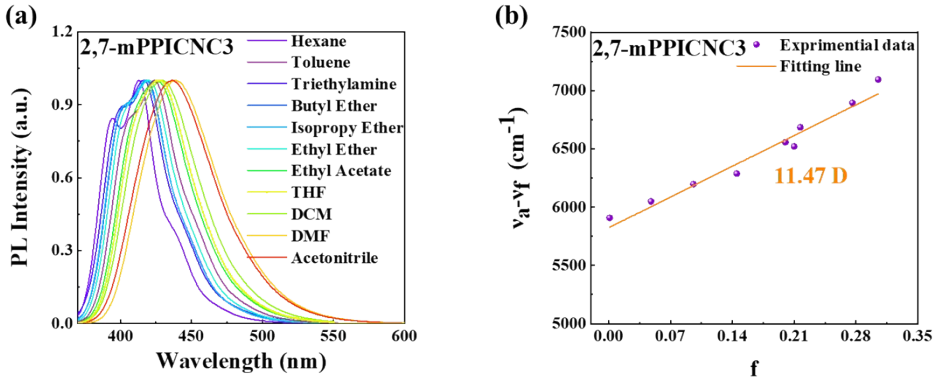

Figure S13. Solvation effects on PL spectra (a) and Lippert-Mataga plots (b) of **2,7-mPPICNC3**.

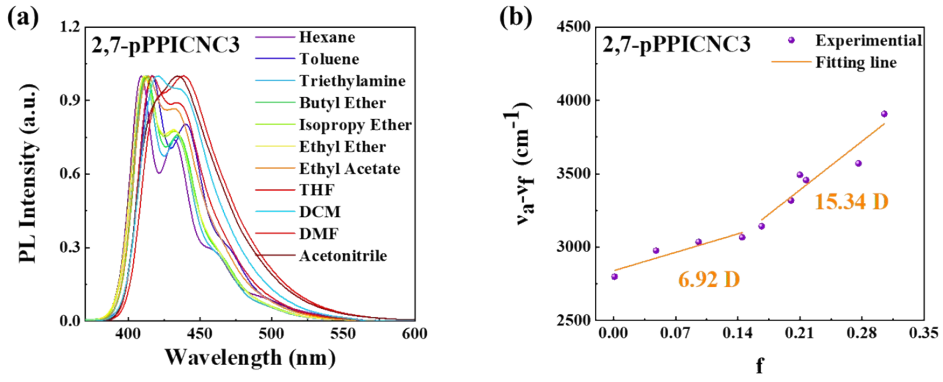

Figure S14. Solvation effects on PL spectra (a) and Lippert-Mataga plots (b) of **2,7-pPPICNC3**.

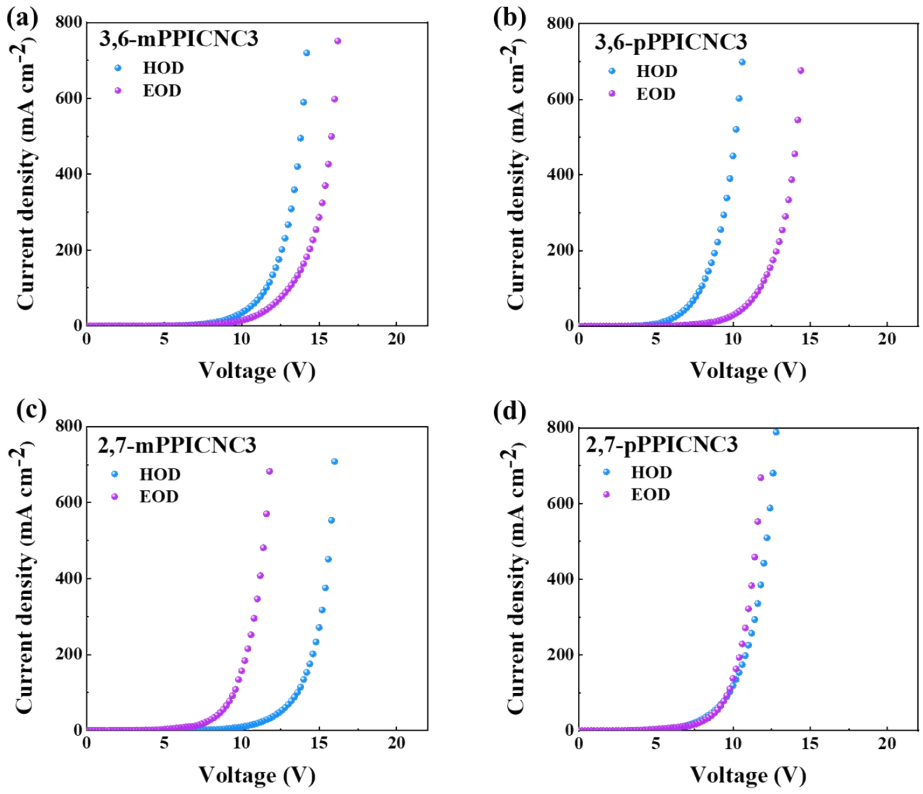

Figure S15. Current density versus voltage curves of the hole-only and electron-only devices of (a) **3,6-mPPICNC3**, (b) **3,6-pPPICNC3**, (c) **2,7-mPPICNC3** and (d) **2,7-pPPICNC3**.

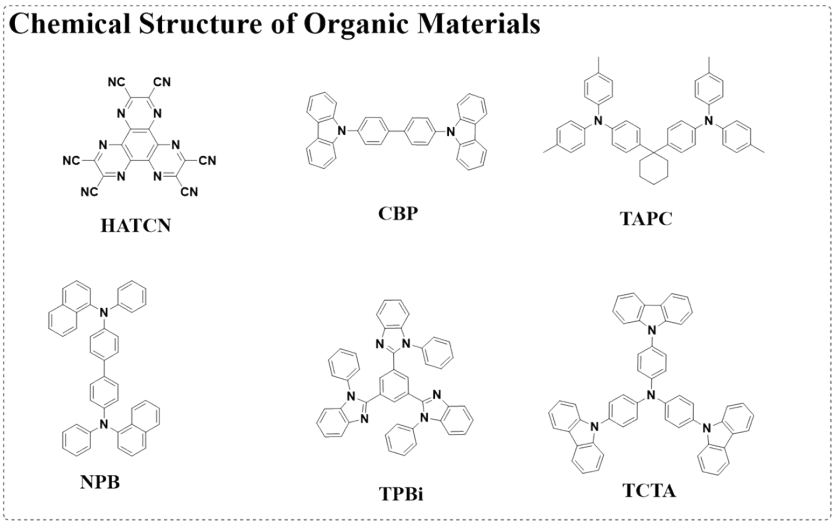

Figure S16. Chemical structure of organic materials used in this work.

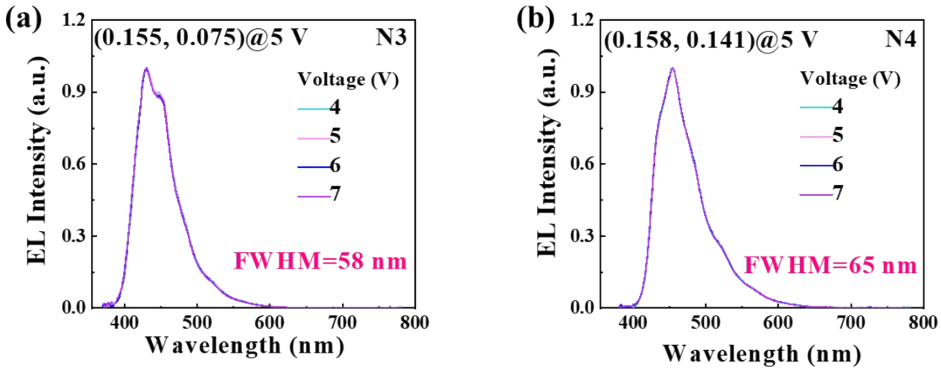

Figure S17. Normalized EL spectra at different applied voltages of the devices (a) **N3**, (b) **N4**.

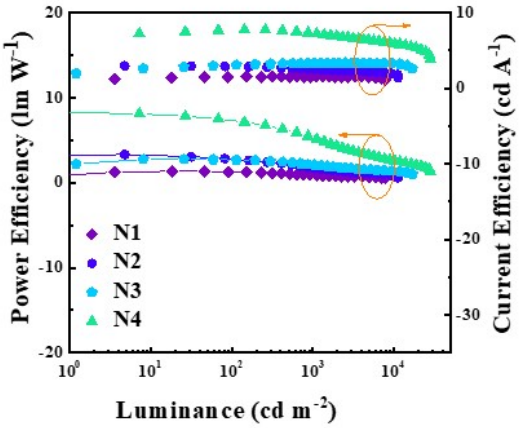

Figure S18. Power efficiency-luminance-current efficiency curves of the devices **N1-4**.

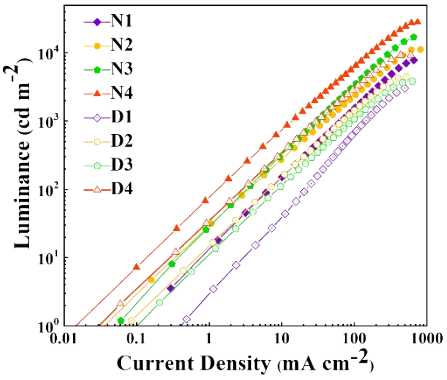

Figure S19. Current density−luminance curves of devices N1-4 and D1-4.

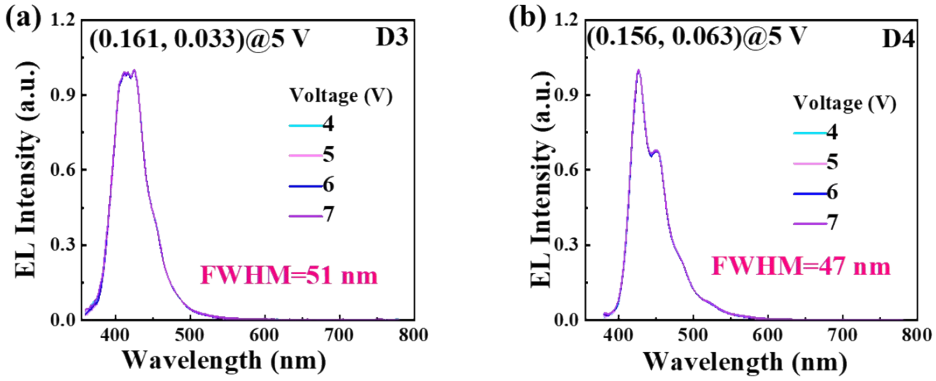

Figure S20. Normalized EL spectra at different applied voltages of the devices (a) **D3** and (b) **D4**.

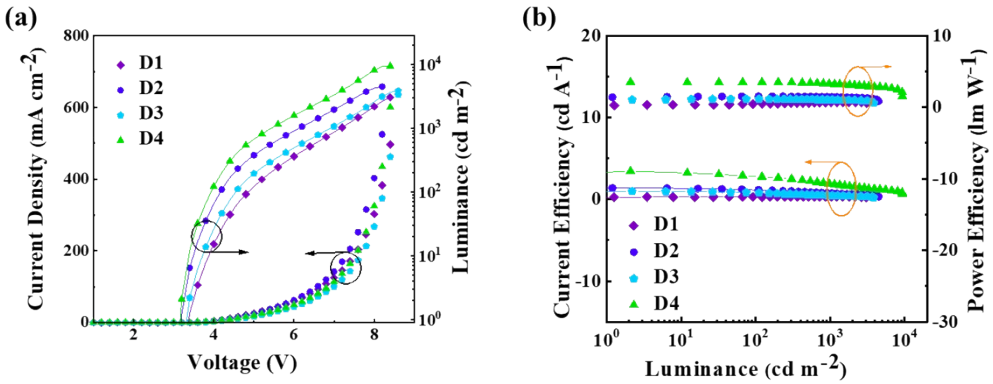

Figure S21. (a) Current density–voltage–luminance characteristics of the devices **D1-4** based on the configurations of ITO/ 1,4,5,8,9,11- hexaazatriphenylenehexacarbonitrile (HATCN, 20 nm)/ 4,4'-(cyclohexane-1,1-diyl)bis(*N,N*-di-p-tolylaniline) (TAPC, 45 nm)/ tris(4-(9H-carbazol-9-yl)phenyl)amine (TCTA, 10 nm)/ 4,4'-bis(*N*-carbazolyl)-1,1'-biphenyl (CBP):Emitter (5 wt%, 20 nm)/ 1,3,5-tris(1-phenyl-1H-benzo[d]imidazol-2-yl)benzene (TPBi, 10 nm)/ LiF (1 nm)/ Al (100 nm). (b) Power efficiency-luminance-current efficiency curves of the devices **D1-4**.

Table S11. Summary of highly efficient violet-blue non-doped and doped (D) fluorescent OLEDs with the CIEy small than 0.05 reported in recent years.

Compound	EQE_{max} [%]	EQE_{1000} [%]	FWHM [nm]	EL Peak [nm]	CIE(x,y)	Ref.
3,6-mPPICNC3	7.67	7.65[a]	44	412	(0.160, 0.032)	This work
3,6-mPPICNC3 (D)	7.85	7.48	41	391	(0.161, 0.025)	This work
POPCN-CP	5.3	2.3	51	404	(0.160, 0.034)	1
POPCN-2CP	7.5	6.1	52	404	(0.159, 0.035)	1
POPCN-2CP (D)	8.2	5.7	50	404	(0.161, 0.034)	1
mTPA–PPI	3.33	-	-	404	(0.161, 0.049)	2
PITZF (D)	6.07	4.88	55	411	(0.159, 0.049)	3
PITZtCz (D)	7.21	6.15	61	413	(0.158, 0.050)	3
PI-TAZ-tbuCZ (D)	6.01	5.10	52	407	(0.160, 0.043)	4
TPBCzC1	4.34	-	-	422	(0.160, 0.035)	5
DCZ2F	5.62	4.23	47	404	(0.163, 0.038)	6
CTPPI	8.10	4.2	-	403	(0.160, 0.040)	7
DSiTPI (D)	7.40	-	-	396	(0.160, 0.050)	8
CSiTPI (D)	5.20	-	-	388	(0.160, 0.050)	8
TBOSi (D)	9.15	-	-	414	(0.165, 0.034)	9
TBOSiCz (D)	8.91	-	-	414	(0.163, 0.031)	9
SBF-PI-SBF	6.19	5.75	64	436	(0.155, 0.049)	10
FIP-CZ (D)	10.4	7.3	49	427	(0.158, 0.039)	11
TPBCzC1	4.34	-	-	438	(0.159, 0.035)	12
Cz-2pbb (D)	2.90	-	-	410	(0.16, 0.05)	13
2MCz-CNMCz	7.76	5.61	-	404	(0.158, 0.039)	14
ICZ-TAZ (D)	4.02	-	46	406	(0.162, 0.037)	15
2BuCz-CNCz	5.24	-	-	408	(0.157, 0.050)	16
2BuCz-CNCz (D)	10.79	6.80		396	(0.161, 0.031)	17
CSP-Bu (D)	6.70	3.69	57	404	(0.158, 0.043)	17
CSP-OMe (D)	7.32	4.75	58	406	(0.158,0.047)	17
VDMP-36PhCz	6.27	4.28	46	402	(0.161,0.043)	18
VDMP-36PhCz (D)	7.55	5.37	50	404	(0.159,0.039)	18
TTT-TPA-H (D)	10.54	-	-	426	(0.15, 0.05)	19
SPA-DBS (D)	1.02	-	55	428	(0.16, 0.04)	20
TFPy4 (D)	5.10	-	54	404	(0.16, 0.02)	21
2Na-CzCN (D)	6.15	5.73	36	392	(0.16, 0.04)	22
mP2MPC	6.09	5.56	51	395	(0.163, 0.028)	23

[a] Recorded at 3300 cd m^{-2}.

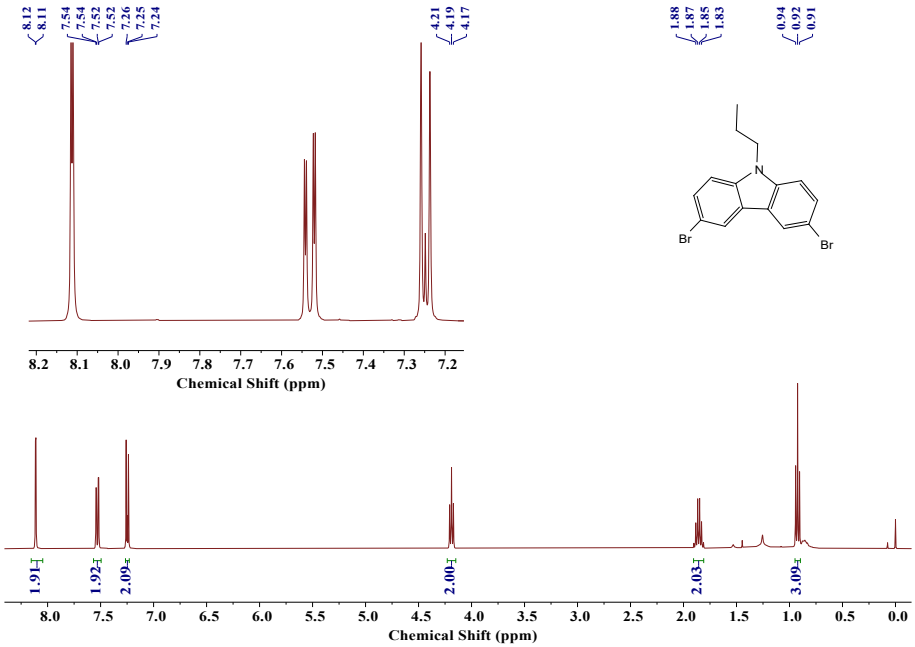

Figure S22. ^{1}H NMR spectrum of **3,6-Br-C3Cz** in $CDCl_3$.

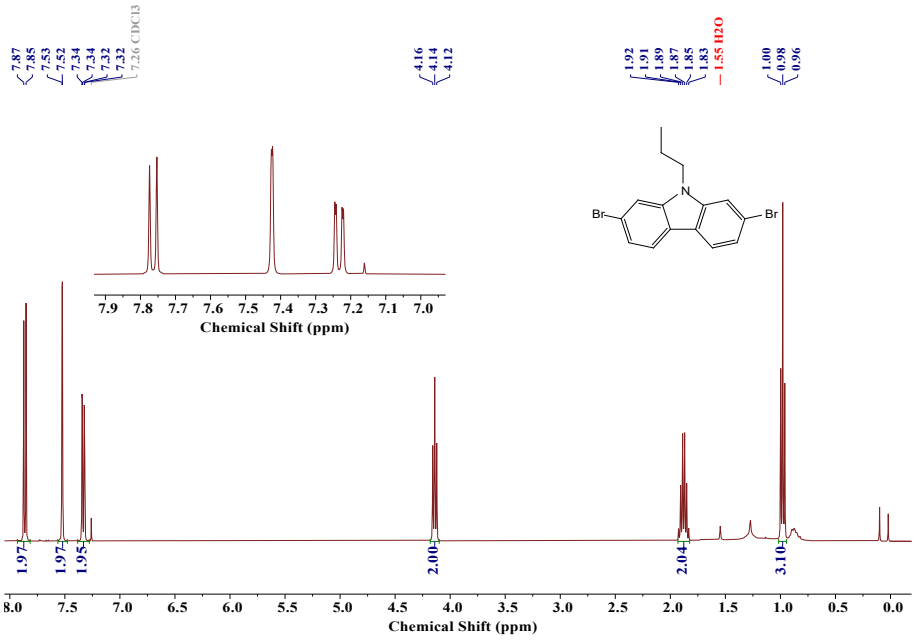

Figure S23. ^{1}H NMR spectrum of **2,7-Br-C3Cz** in $CDCl_3$.

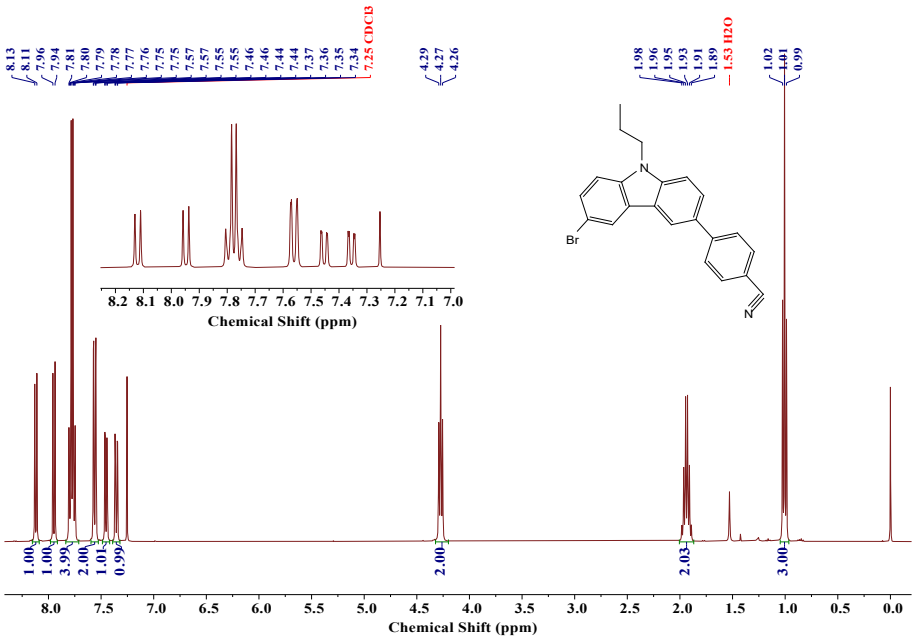

Figure S24. ^{1}H NMR spectrum of **3,6-CNC3** in $CDCl_3$.

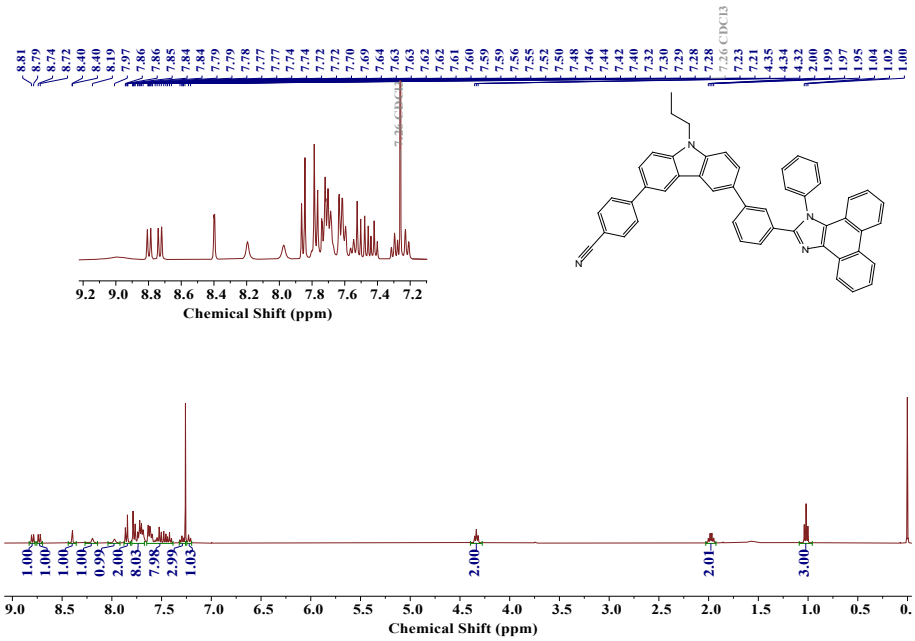

Figure S25. ^{1}H NMR spectrum of **3,6-mPPICNC3** in $CDCl_3$.

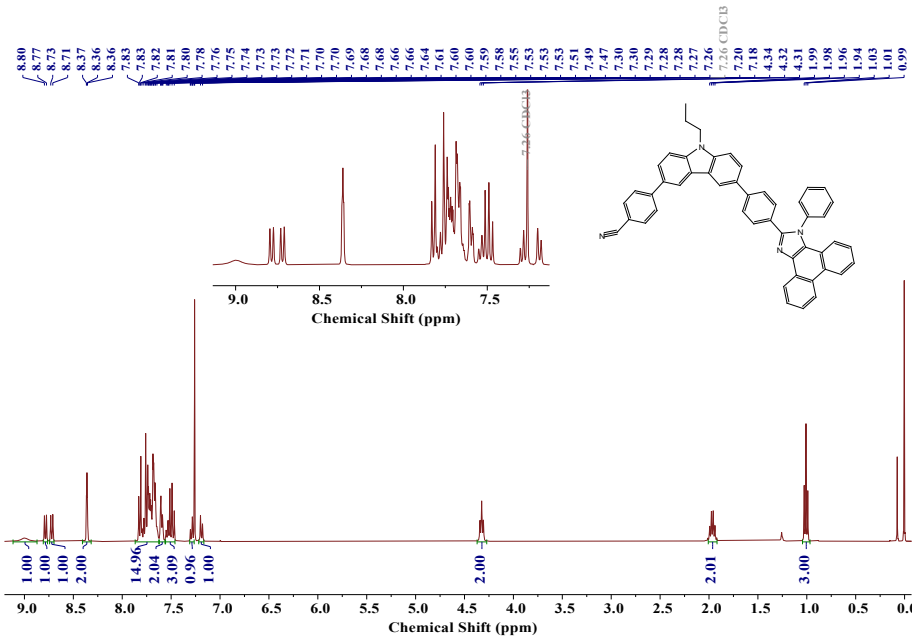

Figure S26. ^{1}H NMR spectrum of **3,6-pPPICNC3** in $CDCl_3$.

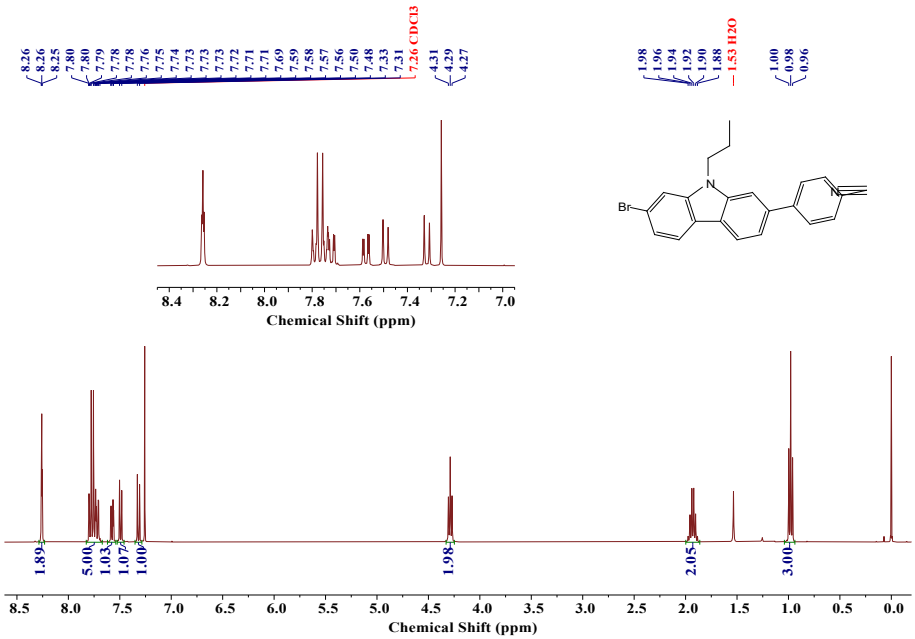

Figure S27. ^{1}H NMR spectrum of **2-CNC3** in $CDCl_3$.

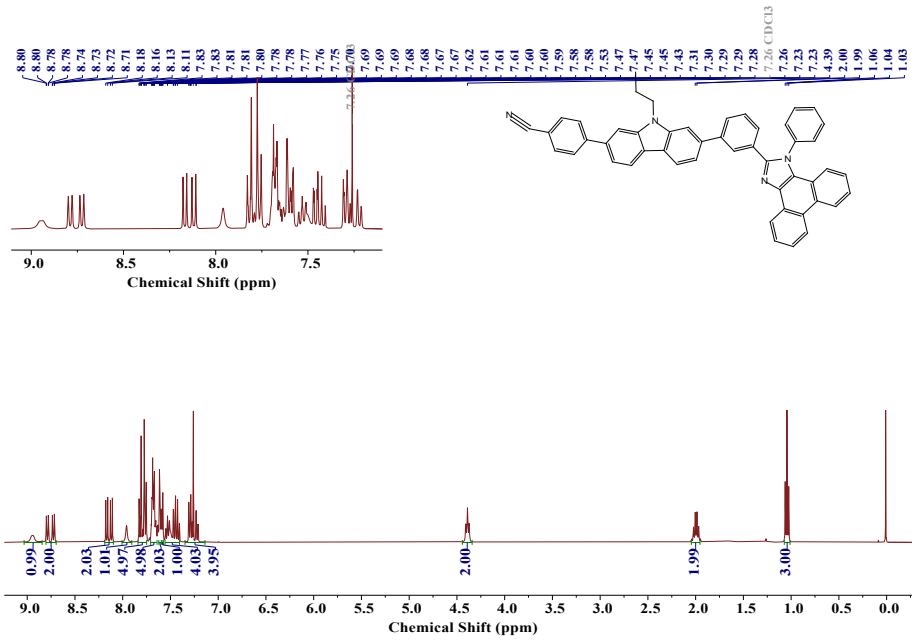

Figure S28. ^{1}H NMR spectrum of **2,7-mPPICNC3** in $CDCl_3$.

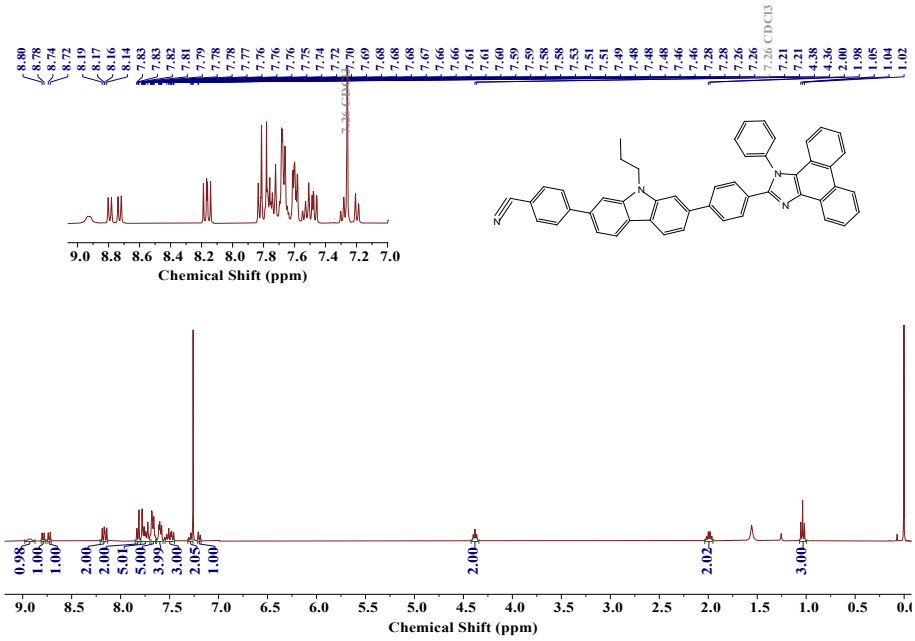

Figure S29. ^{1}H NMR spectrum of **2,7-pPPICNC3** in $CDCl_3$.

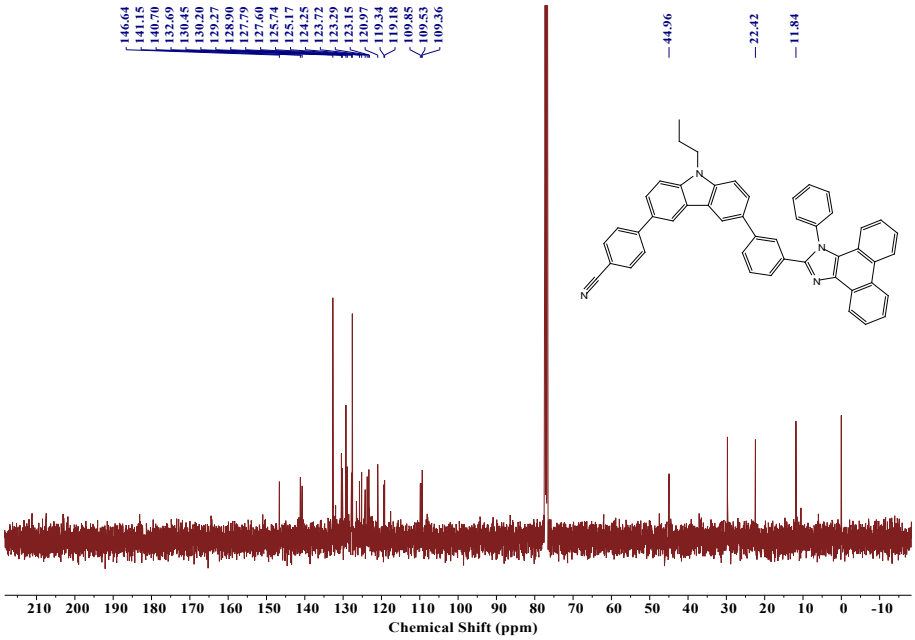

Figure S30. ^{13}C NMR spectrum of **3,6-mPPICNC3** in $CDCl_3$.

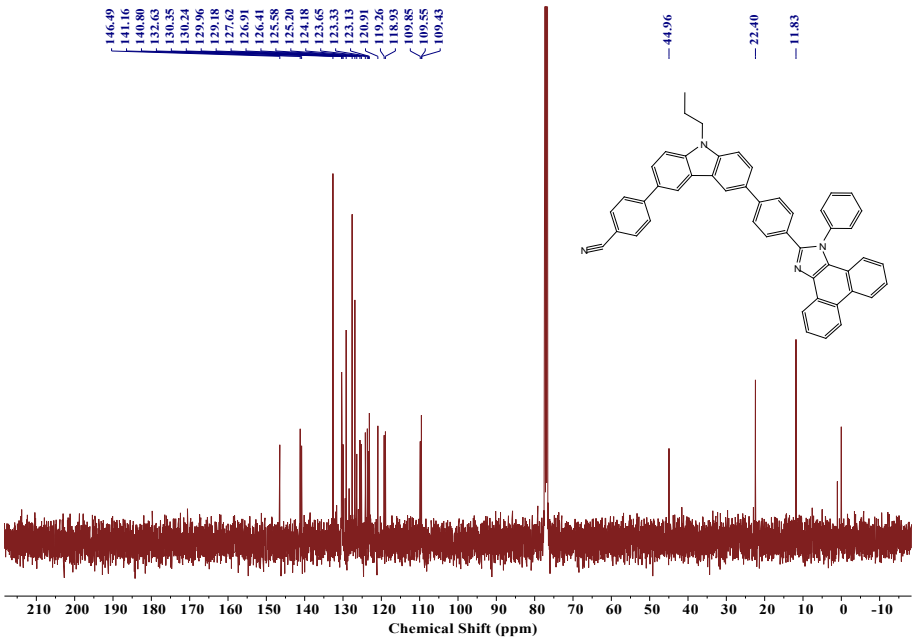

Figure S31. ^{13}C NMR spectrum of **3,6-pPPICNC3** in $CDCl_3$.

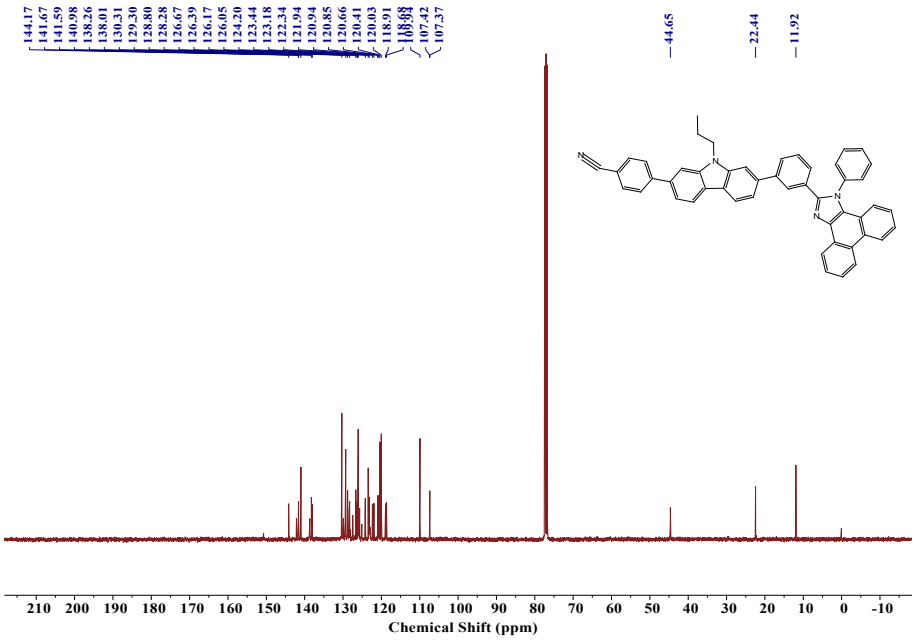

Figure S32. ^{13}C NMR spectrum of **2,7-mPPICNC3** in $CDCl_3$.

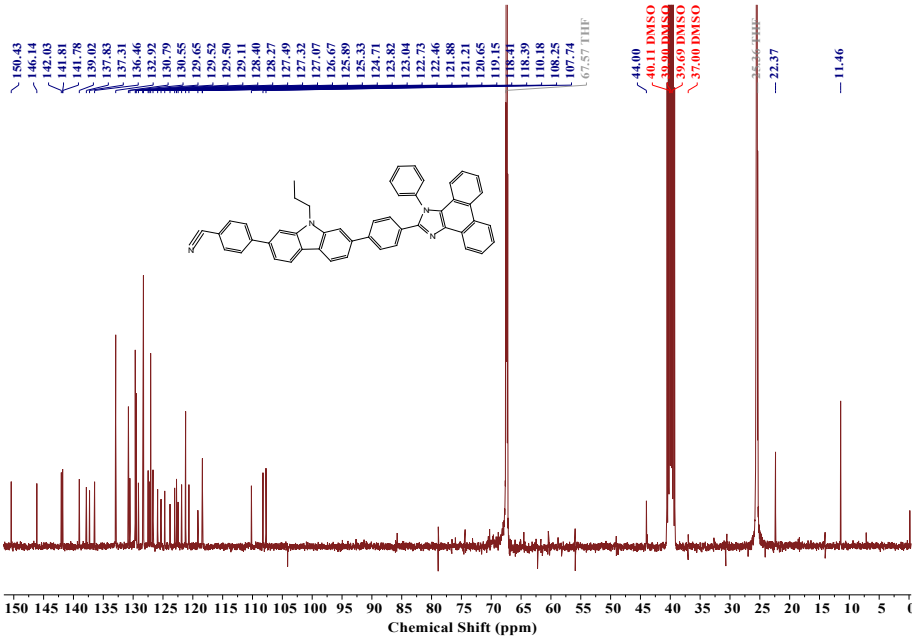

Figure S33. ^{13}C NMR spectrum of **2,7-pPPICNC3** in DMSO-*d*.

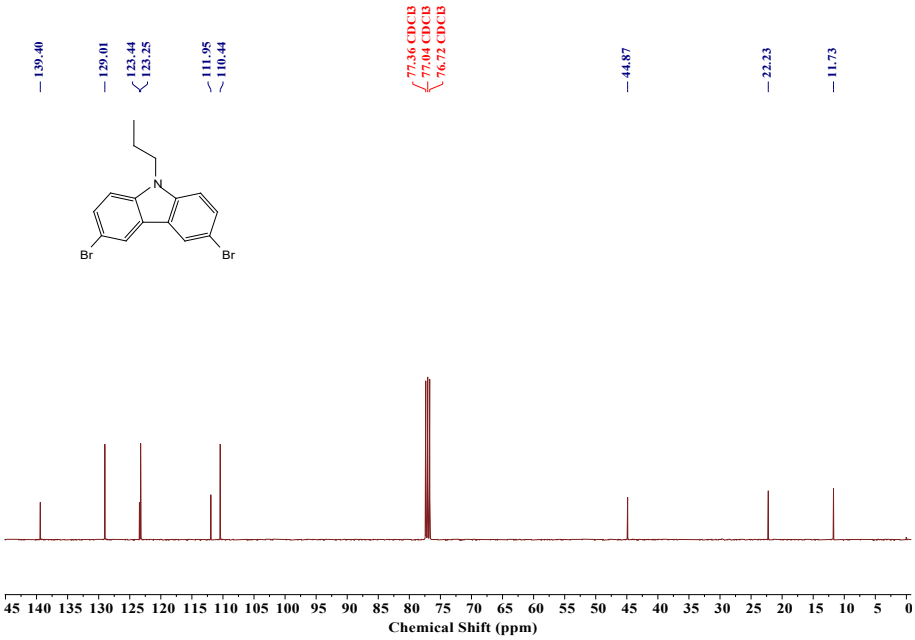

Figure S34. ^{13}C NMR spectrum of **3,6-Br-C3Cz** in $CDCl_3$.

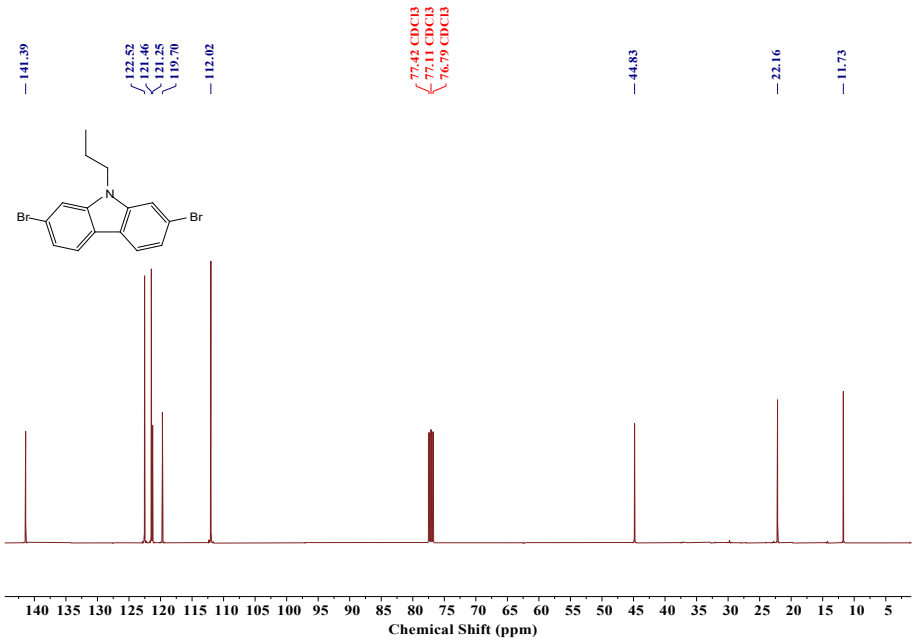

Figure S35. ^{13}C NMR spectrum of **2,7-Br-C3Cz** in $CDCl_3$.

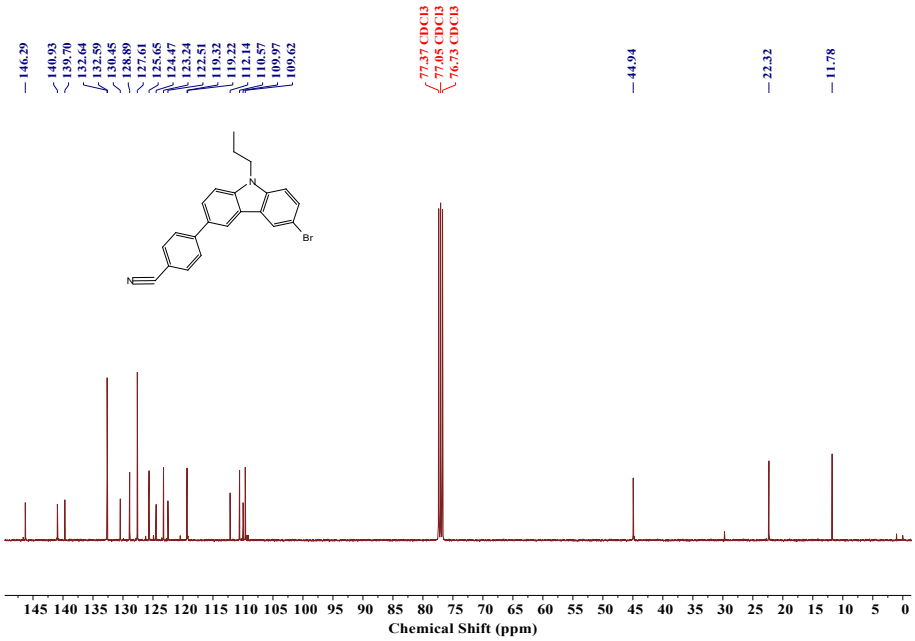

Figure S36. ^{13}C NMR spectrum of **3,6-CNC3** in $CDCl_3$.

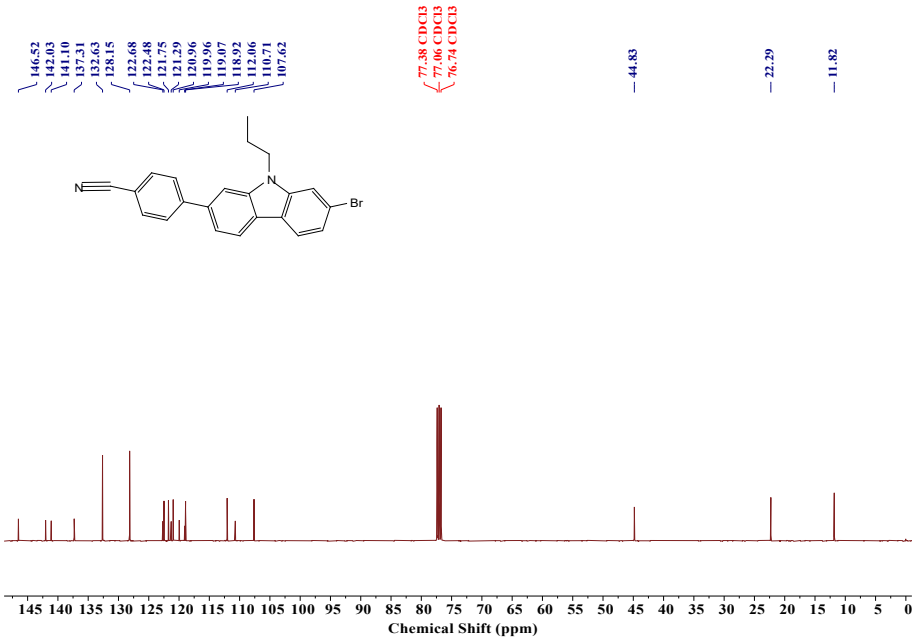

Figure S37. ^{13}C NMR spectrum of **2-CNC3** in $CDCl_3$.

References

[1] J. Chen, H. Liu, J. Guo, J. Wang, N. Qiu, S. Xiao, J. Chi, D. Yang, D. Ma, Z. Zhao, B. Z. Tang, *Angewandte Chemie International Edition* **2022**, 61, e202116810.

[2] H. Liu, Q. Bai, L. Yao, H. Zhang, H. Xu, S. Zhang, W. Li, Y. Gao, J. Li, P. Lu, H. Wang, B. Yang, Y.

Ma, *Chemical Science* **2015**, 6, 3797.

[3] L. Peng, J. Lv, Y. Huo, L. Hua, Y. Liu, S. Ying, S. Yan, *Dyes and Pigments* **2022**, 206, 110676.

[4] L. Peng, Y. Huo, L. Hua, J. Lv, Y. Liu, S. Ying, S. Yan, *Journal of Materials Chemistry C* **2022**, 10, 9621.

[5] P. Han, C. Lin, D. Ma, A. Qin, B. Z. Tang, *ACS Applied Materials & Interfaces* **2020**, 12, 46366.

[6] Y. Huo, J. Lv, M. Wang, Z. Duan, H. Qi, S. Wang, Y. Liu, L. Peng, S. Ying, S. Yan, *Journal of Materials Chemistry C* **2023**, 11, 6347.

[7] Z. Zhong, X. Zhu, X. Wang, Y. Zheng, S. Geng, Z. Zhou, X. J. Feng, Z. Zhao, H. Lu, *Advanced Functional Materials* **2022**, 32, 2112969.

[8] Y. Zheng, X. Zhu, Z. Ni, X. Wang, Z. Zhong, X. J. Feng, Z. Zhao, H. Lu, *Advanced Optical Materials* **2021**, 9, 2100965.

[9] X. Q. Gan, Z. M. Ding, D. H. Liu, W. Q. Zheng, B. Ma, H. Zhang, X. Chang, L. Wang, Y. Liu, X. Wu, S. J. Su, W. Zhu, *Advanced Optical Materials* **2023**, 11, 2300195.

[10] S. S. Tang, G. X. Yang, J. J. Zhu, X. He, J. X. Jian, F. Lu, Q. X. Tong, *Chemistry – A European Journal* **2021**, 27, 9102.

[11] C. Liao, B. Chen, Q. Xie, X. Li, H. Liu, S. Wang, *Advanced Materials* **2023**, 35, 2305310.

[12] P. Han, A. Qin, B. Z. Tang, *Chemical Research in Chinese Universities* **2021**, 37, 16.

[13] X. Yang, S. Zheng, R. Bottger, H. S. Chae, T. Tanaka, S. Li, A. Mochizuki, G. E. Jabbour, *The Journal of Physical Chemistry C* **2011**, 115, 14347.

[14] X. Guo, G. Li, J. Lou, K. Chen, R. Huang, D. Yang, H. Zhang, Z. Wang, B. Z. Tang, *Small* **2022**, 18, 2204029.

[15] X. He, J. Lou, B. Li, H. Wang, X. Peng, G. Li, L. Liu, Y. Huang, N. Zheng, L. Xing, Y. Huo, D. Yang, D. Ma, Z. Zhao, Z. Wang, B. Z. Tang, *Angewandte Chemie International Edition* **2022**, 61, e202209425.

[16] H. Zhang, G. Li, X. Guo, K. Zhang, B. Zhang, X. Guo, Y. Li, J. Fan, Z. Wang, D. Ma, B. Z. Tang, *Angewandte Chemie International Edition* **2021**, 60, 22241.

[17] S. Geng, Z. Liu, H. Li, Z. Zhong, X. J. Feng, Z. Zhao, H. Lu, *Advanced Optical Materials* **2023**, DOI: 10.1002/adom.202301344.

[18] T. Chen, J. Lou, H. Wu, J. Luo, D. Yang, X. Qiao, H. Zhang, B. Z. Tang, Z. Wang, *Advanced Optical*

Materials **2023**, DOI: 10.1002/adom.202301053.

[19] S. Zeng, C. Xiao, J. Zhou, Q. Dong, Q. Li, J. Lim, H. Ma, J. Y. Lee, W. Zhu, Y. Wang, *Advanced Functional Materials* **2022**, 32.

[20] C. Brouillac, W.-S. Shen, J. Rault-Berthelot, O. Jeannin, C. Quinton, Z.-Q. Jiang, C. Poriel, *Materials Chemistry Frontiers* **2022**, 6, 1803.

[21] S. N. Zou, X. Chen, S. Y. Yang, S. Kumar, Y. K. Qu, Y. J. Yu, M. K. Fung, Z. Q. Jiang, L. S. Liao, *Advanced Optical Materials* **2020**, 8.

[22] G. Li, B. Li, H. Zhang, X. Guo, C. Lin, K. Chen, Z. Wang, D. Ma, B. Z. Tang, *ACS Applied Materials & Interfaces* **2022**, 14, 10627.

[23] L. Peng, J. Lv, S. Xiao, Y. Huo, Y. Liu, D. Ma, S. Ying, S. Yan, *Chemical Engineering Journal* **2022**, 450.

[24] L. Lu, F. Chen, *J. Comput. Chem.*, **2012**, 33, 580.

[25] F. Neese, *WIREs Computational Molecular Science* **2012**, 2, 73.